Comparative analysis on dissimilar Laser welding of Ti6Al4V and Ni-Ti with Vanadium and Niobium interlayer

by

Saroj Dahal

Submitted in Partial Fulfillment of the Requirements

for the Degree of

Master of Science in Engineering

in the

Mechanical Engineering

Program

YOUNGSTOWN STATE UNIVERSITY

Date of Submission: May, 2023

Comparative analysis on dissimilar Laser welding of Ti6Al4V and Ni-Ti with Vanadium and Niobium interlayer

Saroj Dahal

I hereby release this <**Thesis>** to the public. I understand that this **<Thesis>** will be made available from the Ohio LINK ETD Center and the Maag Library Circulation Desk for public access. I also authorize the University or other individuals to make copies of this thesis as needed for scholarly research.

Signature:

_____

Typed Name, Student Date

Approvals:

_____

Jae Joong Ryu PhD, Thesis Advisor Date

_____

C. Virgil. Solomon PhD, Committee Member Date

_____

Kyosung Choo PhD, Committee Member Date

_____

Salvatore A. Sanders, PhD, Dean, College of Graduate Studies Date

Abstract

This thesis presents a comparative analysis of the dissimilar laser welding of Ti6Al4V and Ni-Ti with two different interlayers, namely vanadium and niobium, using a continuous fiber laser welding machine. This study attempts to solve the problem associated with dissimilar welding of the Ni-Ti and Ti6Al4V with the use of interlayers specimen. The objective of this study is to improve the welding strength between Ni-Ti and Ti6Al4V in comparison to previous research and to investigate the effect of interlayer composition on the quality of the weld joint. The welding process was performed using identical laser power, welding speed, and focal position, and the quality of the weld joint was evaluated through scanning electron microscopy (SEM), energy-dispersive X-ray spectroscopy (EDS) analysis, hardness testing, and tensile testing.

The welding was successfully performed using both interlayers. The tensile strength of the welded samples with niobium interlayer was found to be 100 MPa greater than that of the samples with vanadium interlayer. Scanning electron microscopy images showed that the fracture occurred at the welding region interface between the Ni-Ti-interlayer in both cases due to the dendritic structure, which caused the region to be more brittle. Furthermore, the hardness of the Ni-Ti-interlayer interface was higher, resulting in brittle fracture at the same interface in both cases during tensile testing.

The findings suggest that the use of niobium interlayer produces a higher quality weld joint with improved mechanical properties under the same laser welding parameters compared to the vanadium interlayer. These results are significant for designing the laser

welding process and selecting the appropriate interlayer for specific applications. Further research can be conducted to optimize the laser welding parameters and explore the impact of different interlayer thicknesses on the welding behavior.

Acknowledgement

I would like to express my deepest gratitude to my thesis advisor, Dr. Jae Joong Ryu, for his invaluable guidance and unwavering support throughout my research. Whenever I faced challenges or felt stuck, Dr. Ryu was always there to provide insightful input and help me find a way forward.

I am also deeply thankful to Taylor Winfield for providing us with access to their Laser Machine, without which our project would not have been possible. I particularly want to express my appreciation to Mr. Mike Gaskill from the research and development department for generously sharing his time and expertise with me. Additionally, I am grateful to Mr. Frank Deley for his assistance in preparing the samples for welding.

I would also like to extend my gratitude to Dr. C. Virgil Solomon and Mr. Ray Hoff for their invaluable contributions to the SEM and EDS analysis of my samples. Dr. Bharat Yelamanchi's support and guidance in using the nanoindentation machine were also instrumental in my research. I am also thankful to Dr. Kyosung Choo for his expert advice on heat transfer analysis during welding.

I want to take a moment to show my gratitude to my loving wife, Surakshya, for always being there for me. Additionally, I would like to extend my heartfelt thanks to my family and friends, Niyam, Sandesh, Sushant, Sahaj, and Mukesh, for their unrelenting support throughout my academic journey.

List of Figures

List of Tables

Nomenclature

SMA	Shape memory Alloy
Ni-Ti	Nickel Titanium
SME	Shape Memory Effect
V	Vanadium
Nb	Niobium
Ni-Ti	Nickel Titanium
σ	Normal stress
HAZ	Heat Affected Zone
Ti6Al4V	Titanium 6Aluminum 4 Vanadium
SEM	Scanning Electron Microscopy
EDS	Electron Discharge Spectroscopy
F	Force
A	Area
GPa	Giga Pascal
MPa	Mega Pascal

Table of Contents

Chapter 1 Introduction

1.1 Background information on Ni-Ti and Ti6Al4V

1.1.1 Properties and Applications

Nickel titanium, also referred to as Ni-Ti, is a shape memory alloy (SMA) with special mechanical characteristics like super-elasticity and shape memory effect (SME) [1]. In addition to having a high strength to weight ratio and excellent corrosion resistance, it is biocompatible [2]. Due to its two-phase structure, which consists of a martensitic phase and an austenitic phase, Ni-Ti can recover its original shape after being deformed [1].

Numerous industries, such as biomedical engineering, aerospace, and energy, have used Ni-Ti [1]. Due to its capacity to recover from deformation, it has been utilized as stents in medical applications [2]. Since it has a shape memory effect and is extremely elastic, Ni-Ti has also been used as actuators in micro-electromechanical systems (MEMS) [1].

Ti6Al4V, also referred to as titanium aluminum vanadium, is a titanium alloy with a high strength-to-weight ratio and exceptional corrosion resistance. It also has a high elasticity modulus and great biocompatibility [3]. The mechanical properties and stability of titanium are enhanced by the addition of aluminum and vanadium [3].

Ti6Al4V is widely used in many industries, including aerospace, medical technology, and sporting goods. It is used in airframes and engine components in the aerospace industry because of its high strength-to-weight ratio and stability at high temperatures [3]. Due to its biocompatibility and high strength, it is utilized in the medical industry for implants, including joint replacements and dental implants [3].

The heat transfer phenomena are another topic of interest in the welding of Ni-Ti and Ti6Al4V because of its effect on the quality of welding. Ni-Ti being shape memory alloy, it has adverse effect after the heat input of such high intensity during welding. Similarly, Ti6Al4V is also affected by high temperature causing the change in microstructure, hence affecting the welding.

1.1.2 Challenges in laser welding of Ni-Ti and Ti6Al4V

The primary difficulty in laser welding Ni-Ti and Ti6Al4V is controlling the heat input and avoiding overheating, which can lead to thermal damage and degradation of the mechanical properties of the alloys [4]. Due to shape memory effect and high thermal conductivity of Ni-Ti, it can be challenging to regulate the heat input during welding, which can result in the formation of unwanted phases and deformation [4]. The shape memory effect also causes distortion causing in the formation of cracks in the weld zone. Furthermore, during laser welding, the high reactivity of Ti6Al4V with nitrogen, oxygen, and hydrogen can lead to the formation of brittle intermetallic and the degradation of mechanical properties [4]. Titanium, being the most reactive element of the periodic table reacts with Nickel to form Ti2Ni, Ni3Ti [5]. Transverse cracks appear in the weld region because of the formation of brittle intermetallic phases as a result [5].

1.2 Research objective and questions

This research focuses on the improvement of weld strength and quality between Ni-Ti and Ti6Al4V. The joining of Ni-Ti and Ti6Al4V have been attempted by many

researchers with different interlayers between them but there has not been any significant change in their welding strength and quality. Based on various research papers, the comparative analysis on laser welding of Ni-Ti and Ti6Al4V using two different interlayers of Vanadium and Niobium. Heat dissipation in two parent materials and interlayer during the welding will also be studied to understand its impact. The strength of the weld will be determined by tensile test and other properties will be investigated by SEM and nanoindentation.

1.3 Significance of the research

The defect free joining of Ni-Ti and Ti6Al4V is a subject of interest for many researchers and scientists as the successful welding of these two metal alloys can broaden the application in aerospace, medical and many other industries as well. There have been attempts to weld Ni-Ti and Ti6Al4V with pulsed laser machines but the comparative study of the weld with continuous laser welding machine with two different interlayers has not been done yet. Defect-free laser welding can result in strong, consistent, and uniform bonds between the two alloys, leading to improved mechanical properties and stability of the joint [4]. This is particularly important in applications where the integrity of the joint is crucial, such as in biomedical implants, where the presence of defects can compromise the biocompatibility and functional performance of the device [4]. Additionally, defect-free laser welding can reduce the need for post-weld processing and inspection, leading to lower production costs and increased efficiency [4].

Chapter 2 Literature review

2.1 Overview of continuous laser welding

2.1.1 Principal and process

A continuous laser beam is used in the high-speed continuous laser welding process to join metal components together [8]. The automotive, aerospace, and medical industries, among others, all use continuous laser welding extensively [9]. The idea behind continuous laser welding is to melt the metal at the welding point by using a continuous laser beam. The metal pieces that need to be joined together with a laser are illuminated by the laser's beam, which heats the metal enough to melt it and create a pool of welding [6]. A joint between the metal pieces is created when the welding pool solidifies.

A few variables, such as laser power, welding speed, beam diameter, and shielding gas, affect the weld's quality [7]. Typically, the laser power is adjusted to deliver the necessary heat input for melting the metal components, and the welding speed is adjusted to maintain the right temperature gradient to avoid solidification cracking [8]. According to Rajaram [10], welding processes are protected from oxidation by shielding gases like argon.

2.1.2 Advantages and Limitations

Compared to conventional welding techniques, continuous laser welding has several advantages. In contrast to other welding techniques, it is a high-speed welding process, allowing for quicker welding times [10]. Secondarily, it produces little distortion

and a smaller heat-affected zone (HAZ), which means that less material is impacted by the heat produced during welding and experiences less warping and deformation [8]. Continuous laser welding additionally offers excellent weld quality and joint strength [7].

The ability to join disparate materials with various melting points is one of the primary benefits of continuous laser welding [6]. It can be used, for instance, to join copper to titanium or aluminum to steel. Because lightweight materials like aluminum and titanium are frequently used in the aerospace and automotive industries, this makes it a perfect welding technique.

The limitations of continuous laser welding are also present. Controlling the heat input while welding is one of the main challenges [10]. A weak joint can result from insufficient heat while an excess of heat can cause the base material to melt. Another restriction is the maximum material thickness that can be welded with continuous laser welding. The method works best with materials that are less than 10 mm thick [8].

Continuous laser welding has the additional drawback of needing an experienced operator and a tightly regulated setting. The welding point must have the laser beam precisely focused on it, and the welding area must be free of any impurities that might compromise the weld's quality [9]. Furthermore, the high initial cost of the equipment required for continuous laser welding can be a barrier for small businesses and startups [7].

In conclusion, continuous laser welding has several benefits over conventional welding techniques, including quicker welding times, minimal distortion, and excellent

weld quality. It is constrained by factors like the requirement for a skilled operator, a controlled environment, and a limit on the thickness of the material that can be welded.

2.2 Laser welding on Ni-Ti and Ti6Al4V

2.2.1 Challenges and Solutions

Due to the special characteristics of Ni-Ti and Ti6Al4V, laser welding them presents several difficulties. Since Ti6Al4V has a high melting point and poor thermal conductivity, it is a challenging material to weld. Ni-Ti, on the other hand, exhibits both super elasticity and the shape memory effect [11].

The formation of intermetallic compounds at the interface of the two materials, which can reduce the mechanical properties of the joint and make it more brittle, is one of the main challenges of laser welding Ni-Ti and Ti6Al4V [12]. At high temperatures, the reaction between the titanium and nickel in Ni-Ti and the aluminum and vanadium in Ti6Al4V results in brittle intermetallic compounds such as Ni2Ti and Ti2Ni [11]. Controlling the heat input during the welding process is another difficulty. Too much heat can cause materials to melt and deform, while not enough heat can lead to weak joints.

The use of an interlayer material such as niobium or vanadium can help overcome some of the challenges of laser welding Ni-Ti and Ti6Al4V [13]. The interlayer material can act as a diffusion barrier between the two materials, reducing the formation of intermetallic compounds and improving the quality of the joint. However, the selection and optimization of the interlayer material and thickness can be a complex process [11].

Controlling the heat input during the welding process is another solution. This can be achieved by adjusting the laser power, welding speed, and focus position. A lower laser power and higher welding speed can reduce the heat input and minimize the formation of defects such as cracks and pores [12].

A shielding gas can also help prevent oxidation of the materials during welding. Argon or helium can be used as shielding gases to protect the weld pool and prevent porosity in the joint [11]. The laser beam must be accurately focused on the welding point to prevent damage to the base materials [12].

2.2.2 Previous studies on interlayer materials

The use of interlayers between titanium and titanium alloy Ti6Al4V has been significantly enhancing the quality of welds. Teshome et.al investigated the microstructure, macro segregation, and mechanical properties of dissimilar laser welds between NiTi and Ti6Al4V alloys using a Co interlayer [13]. The results showed that the Co interlayer successfully prevented the formation of brittle intermetallic phases in the weld, resulting in improved mechanical properties. However, some macro segregation of Co was observed, leading to variations in microhardness across the weld zone. The study provides valuable insights for the development of reliable welding techniques for dissimilar metal joints in biomedical applications [13].

They also conducted the welding with Pd interlayer and found out that the presence of Pd reduced the formation of brittle Ti2Ni (Intermetallic Compounds) IMCs and

improved the joint's mechanical properties, resulting in a joint with super elastic behavior [41]. The tensile strength and rupture strain of the Pd-added joint improved more than twofold, reaching 520 MPa and 5.6%, respectively, and the joint demonstrated superelasticity during cyclic tensile testing. The formation of Ti-Pd compounds over Ti2Ni IMC favored their development, leading to improved mechanical performance of the Pd-added joint [41].

Zoeram and his peers also conducted the study aimed to address the challenges associated with dissimilar welding of Ti6Al4V and Ni-Ti alloys, including the formation of brittle intermetallic phases and transverse cracks in the weld metal. By inserting a copper interlayer between the base metals, the study successfully reduced the formation of brittle phases, eliminated transverse cracks, and improved the mechanical properties of the joint [5].

Similarly, study by Oliveira and their peers successfully used Niobium as an interlayer, which acted as a diffusion barrier, to prevent the formation of brittle phases during the joining process, resulting in crack-free welds and high strength joints [14]. These findings suggest that high melting point filler materials can be used to prevent the formation of undesired phases when joining Ni-Ti to dissimilar materials [14].

Chapter 3 Research Methodology

3.1 Materials and Equipment

3.1.1 Ni-Ti and Ti6Al4V samples

For the experiment, Ni-Ti and Ti6Al4V samples were ordered from McMaster car. The physical properties of Ni-Ti and Ti64Al4V is summarized int the table 3.1.1

Table 3.1-1: Properties of Ni-Ti and Ti6Al4V

Property	Ni-Ti	Ti6Al4V
Density (kg/m³)	6450	4430
Melting Point (°C)	1310	1668
Young's Modulus (GPa)	55	110
Thermal Conductivity (W/m·K)	7	6.7
Yield Strength (MPa)	200 - 600	880 - 950
Ultimate Strength (MPa)	500 - 900	880 - 1100
Elongation at Break (%)	up to 8%	10-15%
Biocompatibility	Biocompatible	Biocompatible

The yield strength and ultimate strength of Ni-Ti can be affected by heat treatment. The change in temperature also causes changes in its super elastic properties and shape memory effect of Ni-Ti.

3.1.2 Interlayer materials

Introduction of suitable interlayer in between Ni-Ti and Ti6Al4V has been proven significant to improve the welding. Zoeram and his peers used copper as an interlayer and were able to improve the quality of welds [5]. Similarly, Tomaschuk and Grevey also came

to conclusion that use of vanadium increased the weld strength of the joint between Stainless steel and Ti6Al4V [15].

Niobium and Vanadium are non-reactive to Titanium which prevents the formation of brittle intermetallic compounds [5,15]. Niobium and Vanadium has a melting point of 2477 degree Celsius and 1910 degree Celsius respectively which are higher than the melting point of Ti6Al4V (1668) and Ni-Ti (1310). The higher melting point of the interlayers makes a good fusion between Ni-Ti and Ti6Al4V preventing the diffusion and hence preventing the formation of brittle intermetallic phases. The physical properties of Niobium and Vanadium given in the table:

Table 3.1-2: Properties of Vanadium and Niobium

Property	**Niobium**	**Vanadium**
Density (kg/m³)	8570	6000
Melting Point (°C)	2477	1910
Young's Modulus (GPa)	105	128
Thermal Conductivity (W/m·K)	54.8	30.7
Yield Strength (MPa)	185	550
Ultimate Strength (MPa)	600	800
Elongation at Break (%)	50-70	40
Biocompatibility	Biocompatible	Biocompatible

3.1.3 Laser welding machine

The welding of the materials was performed by the continuous laser welding machine at Taylor Winfield with maximum outpower of 10KW. The machine is a fiber laser machine designed by IPG electronics to weld the metals for a fast-paced environment for industrial setup.

Fiber lasers use optical fibers to amplify and direct a laser beam. A laser beam is generated by a laser diode and transmitted through an optical fiber doped with rare earth elements such as erbium, ytterbium, and neodymium. These elements are added to the fiber during manufacturing to enable the fiber to amplify laser light.

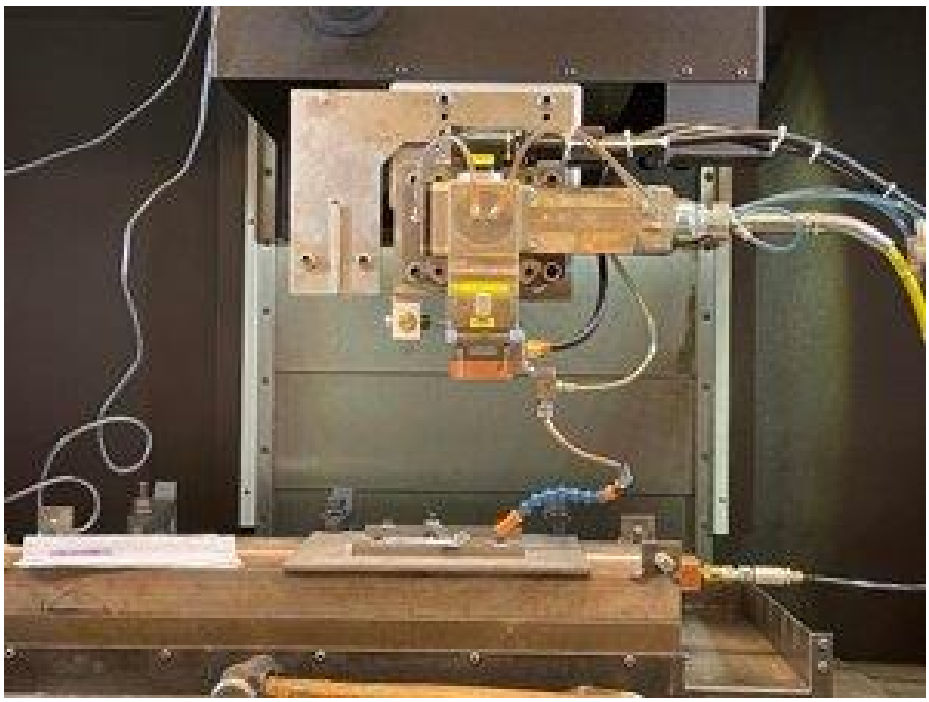

Figure 3.1.1: YLS-1000-C model laser welding machine

3.2 Welding Process

3.2.1 Preparation of welding samples

The samples of parent materials Ni-Ti and Ti6Al4V were cut into pieces using the water jet cutting in Taylor Winfield and the interlayer materials were cut using the shear cutter. The dimension of the sample is 50mm×30mm×2mm.Thge dimension of the interlayer is 1mm×30mm×2mm. The edges of the samples were polished using sandpaper to ensure the elimination of the rough surface for the butt welding. Figure shows the dimensions of the samples.

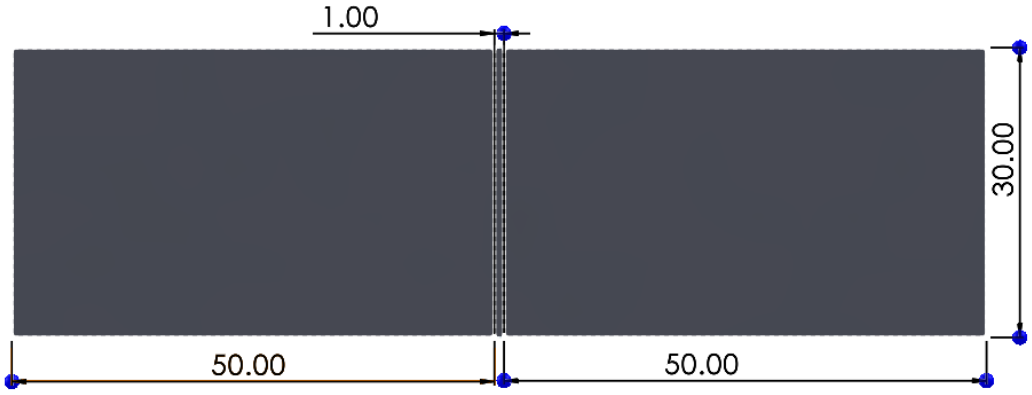

Figure 3.2.1: Sample Dimensions

3.2.2 Welding Setup and Parameters

The welding setup was designed to clamp the samples to restrain any movement. The fixtures were designed in SolidWorks and then machined to build a setup. Figure depicts the comparison between welding setup conceptual design and actual welding setup.

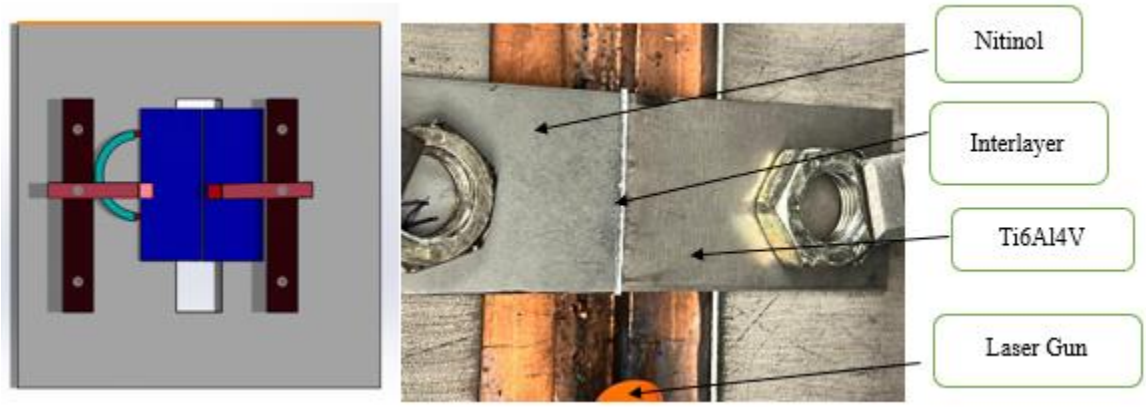

Figure 3.2.2: Welding setup

Determination of the right welding parameters was one of the difficult challenges for the experiment. Various literature reviews and different trials over the period were applied to come up with the right parameters for the welding. Many literatures used the pulsed laser welding machine which were different than the continuous laser machine that was used for the experiment. Dr. Tomaschuck and his peers performed the welding of AISI 306L stainless and Ti6Al4V with the continuous laser welding machine with vanadium interlayer [15]. He and his peers attempted the welding with three different approaches. They were single pass and double pass. After attempting the different trials, the parameters for the welding were determined as shown in the Table 3.2-1.

Table 3.2-1 Welding parameters

Welding speed (mm/sec)	33
Average Laser Power (W)	2000
Defocusing distance	0
Laser beam diameter (mm)	0.5
Voltage (V)	400-480
Argon gas flow	70 CFH

The beam diameter of the laser was 0.5mm and the thickness of the interlayer was 1mm. When the single pass welding was attempted, interlayer was not welded to both parent materials. Therefore, a double pass welding was conducted which resulted in the successful welding. The first pass was made on the Ti6Al4V side and then moved over by 1mm and then second pass was conducted. The argon gas as a shielding gas minimized the oxidation during the welding process.

3.3 Welding Analysis

Firstly, visual analysis of the samples was done to observe if there any visible large cracks are present in the welding region. After visual inspection, it was clear that the crack free welding was achieved. Since improving the welding strength of the weld between two titanium alloys was the primary objective, tensile test was done. The welding zone was captured using the VHX microscopic camera as shown in Figure 4.1.1.

Figure 3.3.1:Keyence high resolution digital microscope

3.3.1 Tensile testing

The strength of the welded samples was analyzed by tensile testing using the Instron 5500R machine. The test was performed based on ASTM E8 standard. The loading rate was 3mm/min. The dimensions of the sample were 100mm×30mm×2mm. The samples were not cut into dog-bone shapes because of the unavailability of the resource to cut the high strength materials such as Ni-Ti and Ti6Al4V. The cross-section area was normalized for the calculation of the stress. Extensometer was used to determine the strain of the gauge length of 50mm. Figure 3.3.1 depicts the process of tensile testing for the samples.

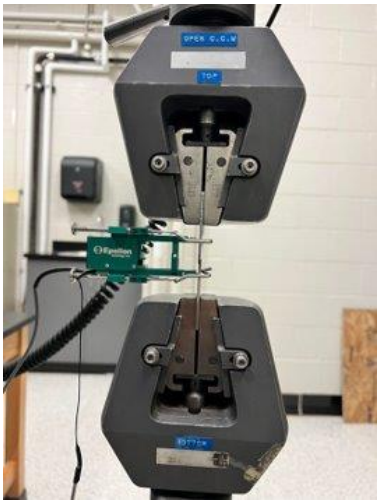

Figure 3.3.2: Tensile testing using Instron 5500 R

The stress and strain calculation were done by using equations 3.1 and 3.2 respectively.

$$\sigma = \frac{F}{A} \tag{3.1}$$

Here, F is the applied tensile load and A is the normalized cross-sectional area of the sample.

$$\varepsilon = \frac{\Delta L}{L} \tag{3.2}$$

Here ε is the strain, ΔL is the change in the length of sample during tensile test and L is the gauge length of the sample.

3.3.2 Sample preparation for microstructure and Hardness analysis

After the tensile test, the welding part of the samples were carefully cut using the shear cutter and embedded in the epoxy for further SEM analysis of the fracture region.

Due to the limited number of samples, broken samples from tensile testing were cut and then welded together with the dimension of 40mm×20mm×2mm and then welded together for the further SEM, EDS, and hardness analysis of welded region. Figure 3.3.3 depicts the prepared and polished samples for the analysis.

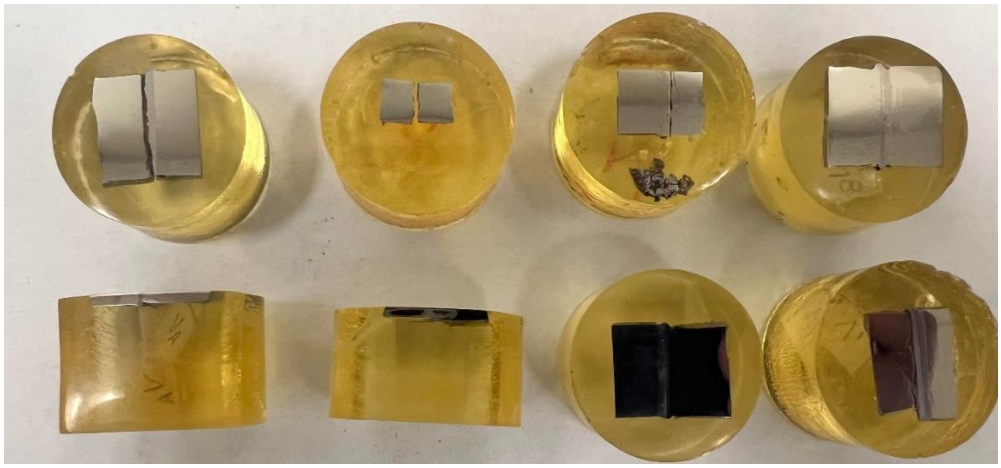

Figure 3.3.3: Polished samples.

3.3.3 Nanoindentation

The hardness of the HAZs and interlayer along with parent materials was calculated using the nanoindentation technique. Figure 3.3.4 depicts the setup to measure the hardness. The parameters for the hardness tests are shown in table 3.3-1.

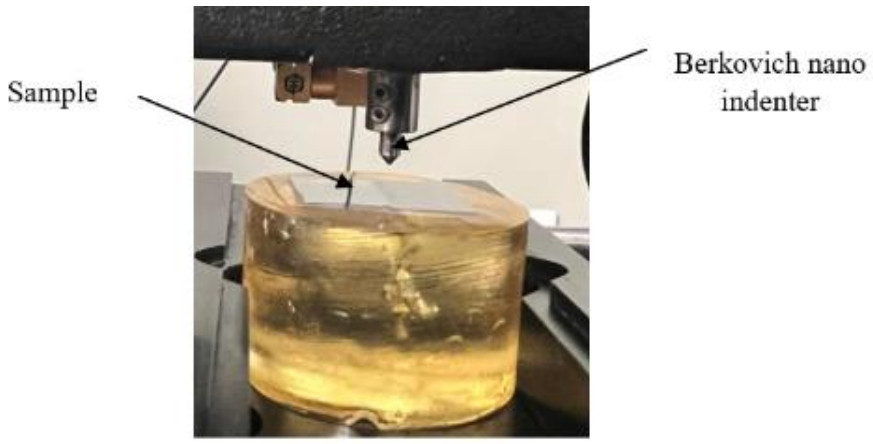

Figure 3.3.4: Nanoindentation test setup

Table 3.3-1: Parameters for nanoindentation analysis

Parameters	**Value**
Approach speed	10 µm/min
Contact load	0.1 mN
Indenter	Berkovich-Be 0070
Load	300 mN
Loading rate	150 mN/min
Unloading rate	150 mN/min

The Berkovich indenter is a popular type of sharp, three-sided pyramid-shaped indenter used for measuring the hardness of materials. The three faces of the pyramid are equilateral triangles with an included angle of 65.28 degree [36]. The loading vs depth curve that is obtained from the indenter is depicted in figure 3.3.3.

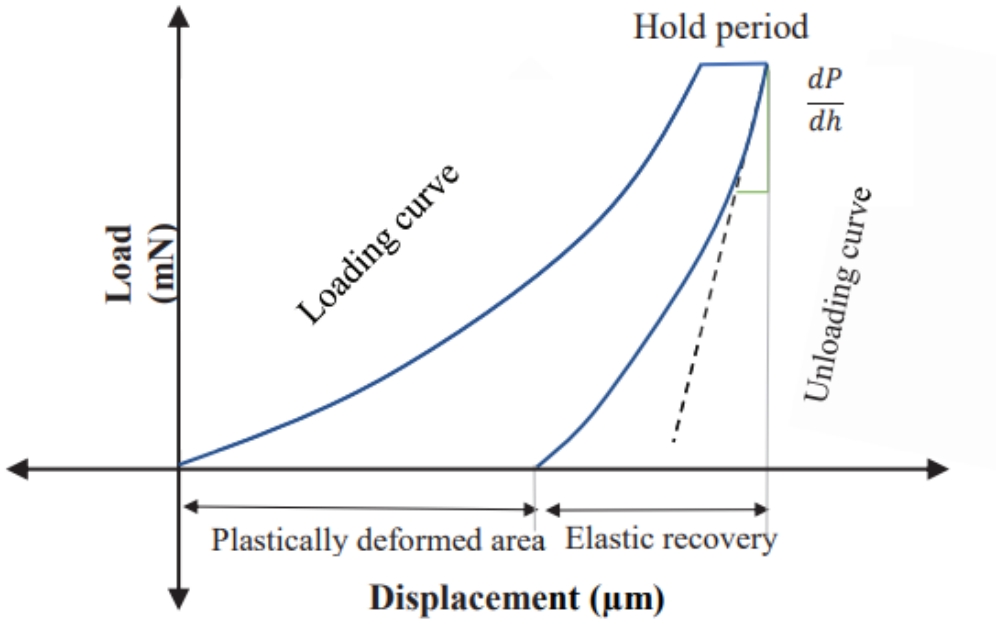

Figure 3.3.5: Loading vs depth curve [35]

The hardness can be calculated by using the formula.

$$H = \frac{P_{max}}{A_c} \tag{3.2}$$

Here, P_{max} is the maximum load applied and A_c is the projected area. Projected area is calculated as:

$$A_c = 3.\sqrt{3}.h^2.(tan\theta)^2 \tag{3.3}$$

Here, 'h' is the penetration depth at maximum load at angle θ which in case this research is 65.28 degrees.

3.3.4 Microstructure Analysis

SEM and EDS analysis of the polished samples were performed for the better understanding of welding region. SEM analysis showed the difference between the welding region, HAZs and parent material region. EDS gave us the understanding of the elemental composition in different regions. The figure depicts the machine used for SEM and EDS of the samples.

Figure 3.3.6:Scanning Electron Microscope

Chapter 4 Results and Discussion

4.1 General welding observations

The welded samples were inspected thoroughly to detect the quality of welding. It was found that both the samples with Vanadium and Niobium interlayer were welded successfully without any cracks. Figure 4.1.2 and figure 4.1.3 depict the welded samples with vanadium and niobium interlayer with their microscopic images respectively.

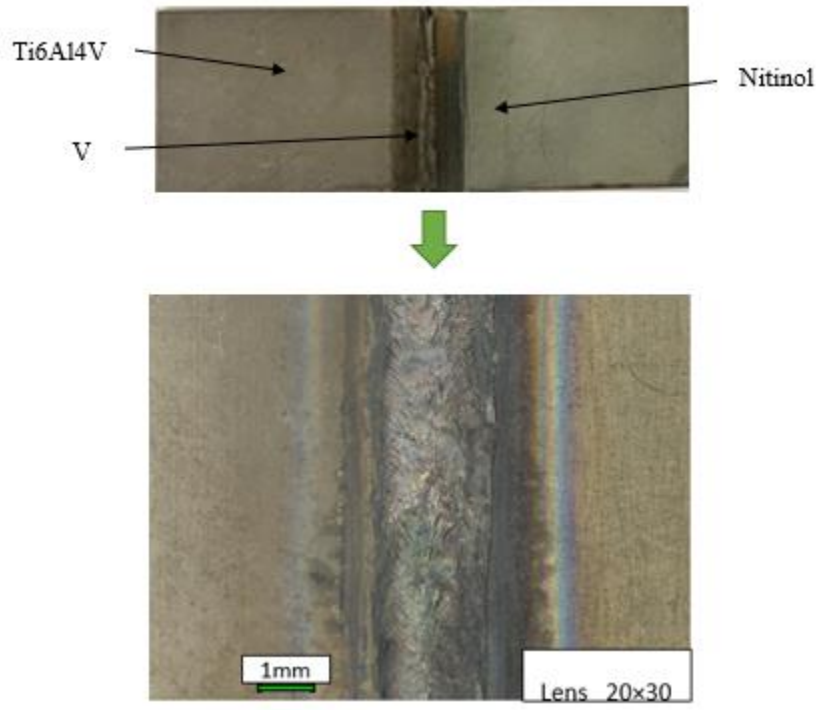

Figure 4.1.1: Welded samples with Vanadium interlayer

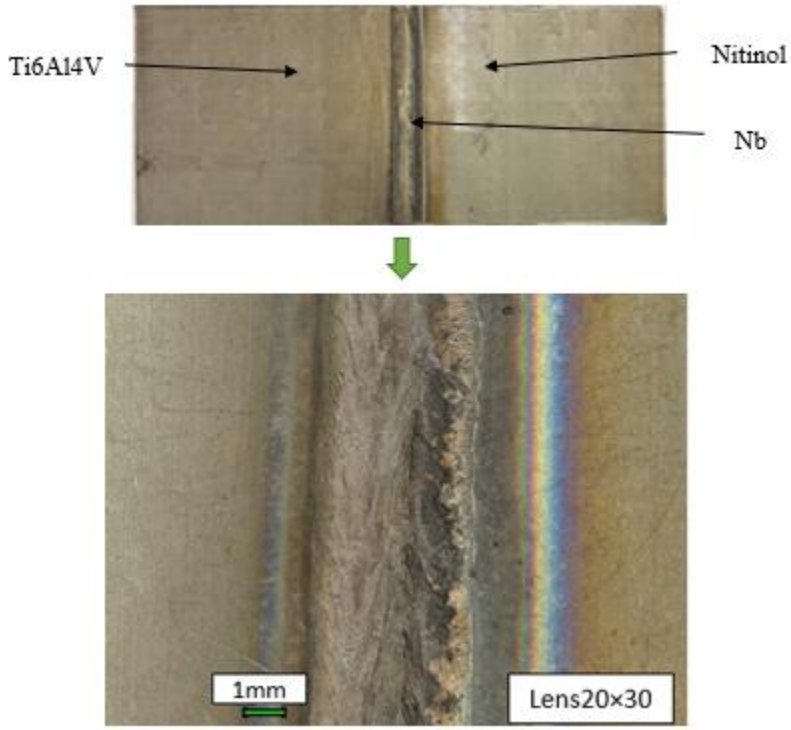

Figure 4.1.2: Welded samples with Niobium interlayer.

As mentioned earlier, due to their high melting point, both Vanadium and Niobium acted as a barrier to the fusion of Ni-Ti and Ti6Al4V during the welding process. Hence, the formation of brittle intermetallic phases is hugely reduced. The microscopic images for both samples with Nb and V interlayer shows that the fusion of the materials takes place without any defect. The interlayer materials in both cases do not melt completely because of their high melting point as compared to the Ti6Al4V and Ni-Ti.

The cross-sectional weld region was also analyzed using the optical microscope. This analysis clarified the weld penetration and the fusion zone across the cross-sectional

region as well. Figure 4.1.3 and 4.1.4 depicts the cross-sectional region of Vanadium and Niobium interlayer samples respectively.

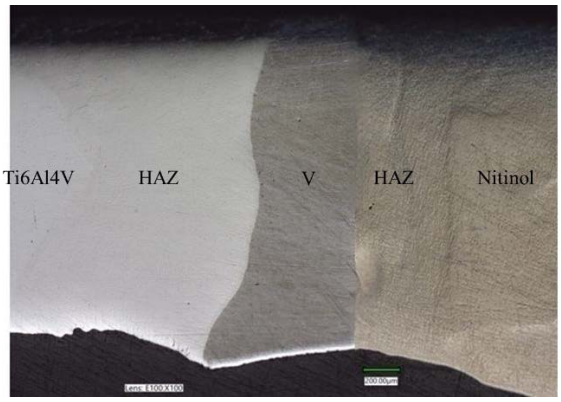

Figure 4.1.3: Cross-sectional region of the Vanadium interlayer sample

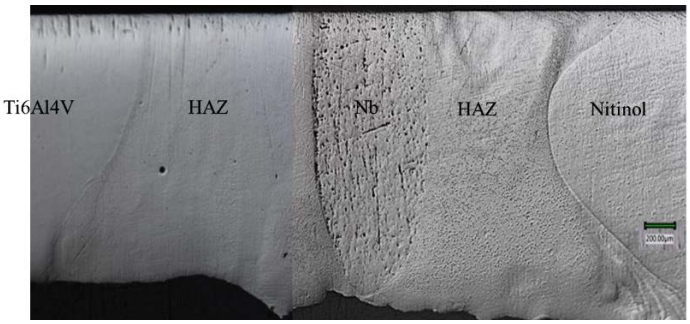

Figure 4.1.4: Cross sectional region of Niobium interlayer sample

The figures depict that the welding performed was able to join the two metals from top to bottom without any discontinuity. Figure 4.1.3 depicts that the HAZ region of Nitinol is less than the HAZ region of Ti6Al4V. This is the result of the involvement of the human precision in the welding process. While moving the beam diameter for the second pass, the offset might be off slightly causing the change in HAZ. In case of figure 4.1.4, the HAZ is uniform in both base alloys.

4.2 Analysis of Vanadium interlayer samples

4.2.1 Tensile test and elongation for samples with vanadium interlayer

The strength of welded samples was determined by the tensile test. The fracture was found to be brittle as no yielding occurred. The maximum tensile strength of the welded sample ranged from 215 MPa to 295 MPa and elongation ranged from 0.048 to 0.069. Figure 4.2.1 illustrates the stress and strain curve for the welded samples with V interlayer.

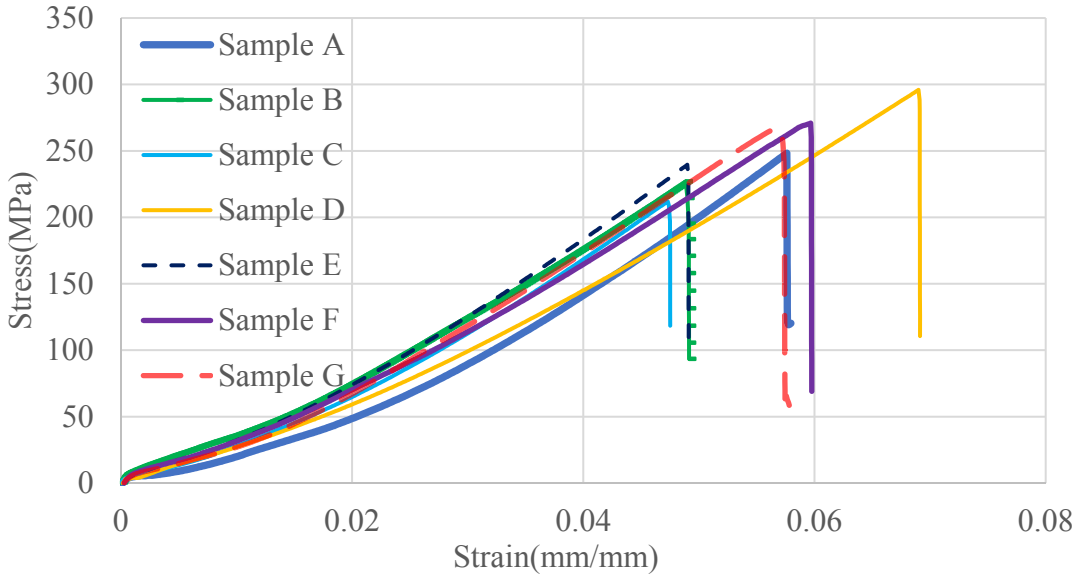

Figure 4.2.1: Stress vs Strain curve for vanadium interlayer samples.

The maximum values obtained for stress and strain for the samples are tabulated in table 4.2-1 and the maximum tensile strength of the different samples are illustrated in the bar diagram in figure 4.2.2.

Table 4.2-1: Maximum stress and strain for vanadium interlayer samples

Sample	Stress	Strain (%)
A	239.58	4.9
B	215.23	4.7
C	243.41	5.7
D	270.44	6.0
E	264.75	5.7
F	235.74	4.8
G	295.93	6.9
Average	**252.15**	**5.4**
SD	**23.12**	**0.5**

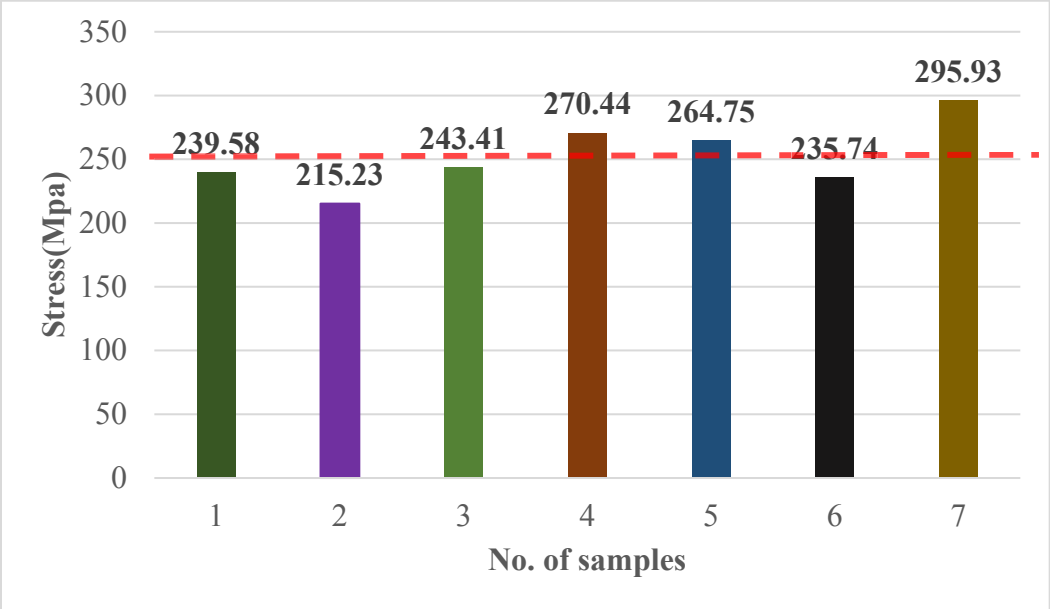

Figure 4.2.2: Maximum tensile strength of V interlayer sample.

A total of seven samples were tested and it was found that none of them had the exact same strength. However, a similar trend of the curve was noted for all the samples. The average strength of all the samples was 252 MPa and average strain was 0.055. There are several factors which cause such a wide range of stress and strain. Every process from

insertion of interlayer, clamping of samples, and directing the laser beam to the samples was manual task. Although every step of each welding trial was conducted carefully, a slight unknown change that is difficult to detect can cause the weld to be of different nature in terms of its strength.

When an attempt to weld Ni-Ti and Ti6Al4V was made initially, the welding could easily be broken with the hand because of its brittleness. Vanadium interlayer made the weld stronger and defect free as compared to the welding without any interlayer. The samples were then observed carefully to determine the region of fracture. From the fractured specimen, it was noticed that the fracture occurred in the Ni-Ti region. Figure 4.2.2 depicts the fractured sample after tensile test.

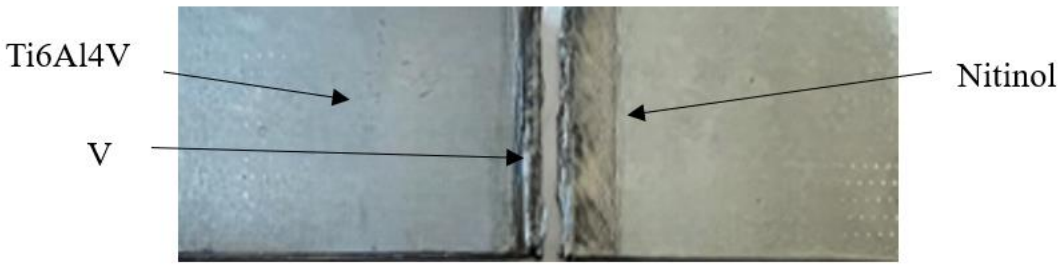

Figure 4.2.3: Broken V interlayer sample after tensile test

The interlayer is not completely melted, and it's attached to Ti6Al4V and completely detached from Ni-Ti. The fracture was observed to be in the interlayer (Ni-Ti-interlayer) side. The SEM analysis was conducted to ensure the region where fracture occurred.

4.2.2 Microstructure analysis for Vanadium interlayer.

After the tensile test, SEM analysis of the samples was done for the better understanding of fracture region. Figure 4.2.3 depicts the overall area of the fracture zone.

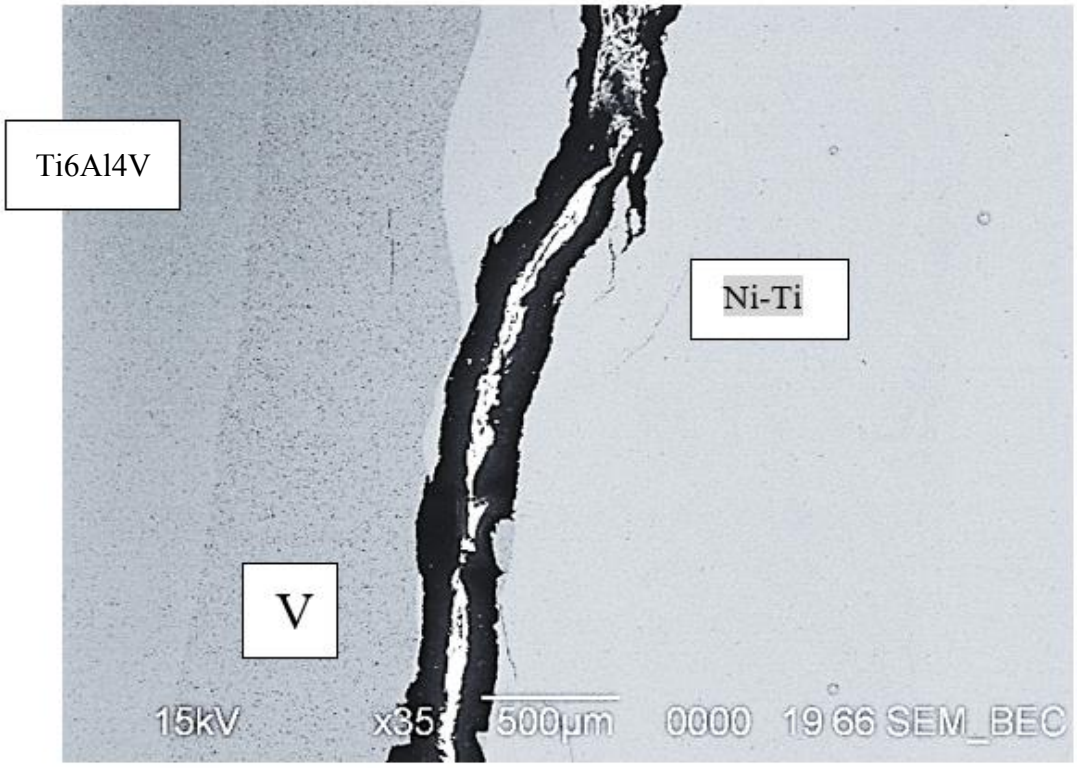

Figure 4.2.4: SEM fracture image after tensile test

From SEM it was confirmed that the sample broke in the HAZ region of Ni-Ti.

Figures 4.2.4 shows the different regions of the welded samples. The fusion between V interlayer and Ti6Al4V was free from transverse cracks. Although, the Ni-Ti and V interlayer were also welded free of cracks, the HAZ of Ni-Ti is where the crack took place. The HAZs were further analyzed to understand their formation and their elemental

composition. Figure 4.2.4 depicts the overall SEM image of the welded zone and formation of HAZS.

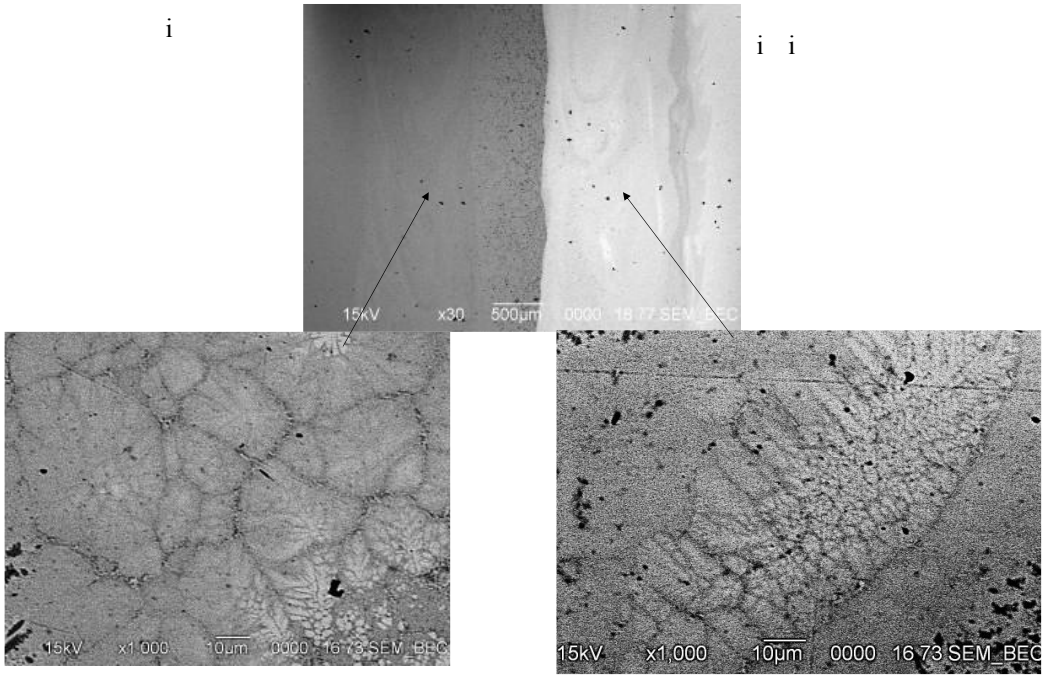

Figure 4.2.5: SEM images of the welded region (Vanadium Interlayer)

To begin the Vanadium is not melted and is in original shape. Vanadium is properly attached to both the parent materials causing the melting zone of the materials difficult to detect. The patterns in the Ti6Al4V side show the two phases (dark and light). The dark phase symbolizes the presence of light element and light phase symbolizes the presence of heavy element.

In the Ni-Ti side of the weld, formation of dendrites structure can be spotted. Zoeram et. al. also found the equiaxed dendrites formation in the Nitinol region due to the

heating and cooling effect [15]. The black spots had Ni2Ti compounds present in them [15].

Further, to determine the elemental composition of the weld region and HAZs, EDS analysis was done. To begin, the EDS analysis was done on the HAZ of Ti6Al4V and Ni-Ti side for the understanding of the elemental composition. Figure 4.2.6 depicts the elemental composition across the interlayer and HAZ regions. And Table 4.2-2 illustrates the elemental composition in the whole region.

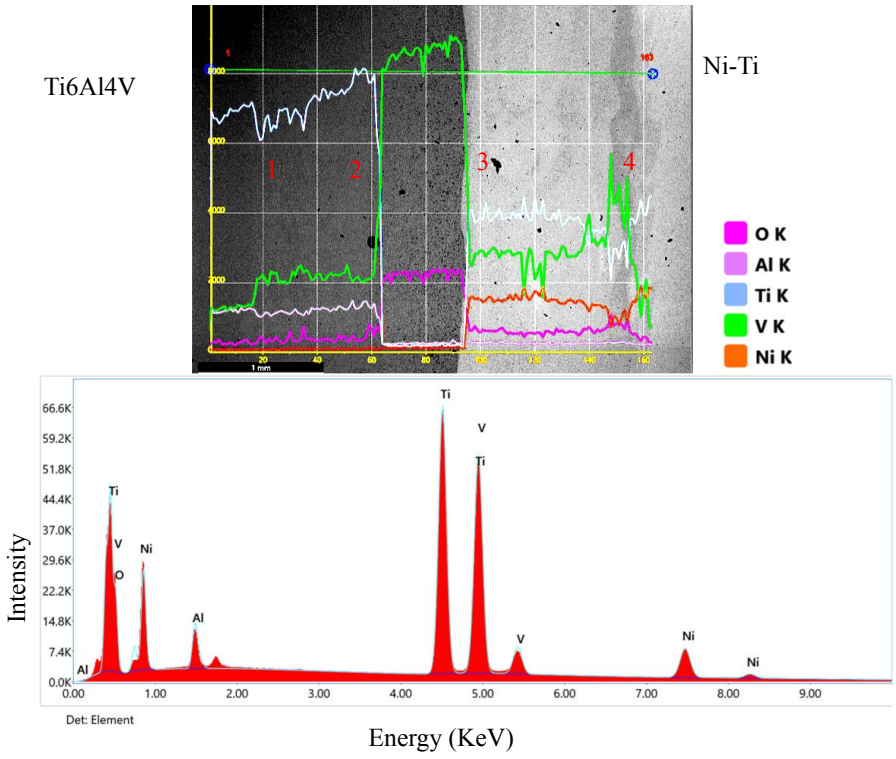

Figure 4.2.6:EDS analysis on V interlayer sample

Table 4.2-2: Elemental Analysis on the HAZs and V interlayer

Zone 1		
Elements	Wt. %	At. %
Al	5.13	8.86
Ti	75.92	73.82
V	18.95	1.44
O	0	0

Zone 2		
Elements	Wt. %	At. %
Al	5.25	8.37
Ti	76.08	68.42
V	13.76	11.63
O	2.71	10.95

Zone 3		
Elements	Wt. %	At. %
Ni	38.38	31.88
Ti	33.31	33.91
V	24.72	23.65
O	3.28	10

Zone 4		
Elements	Wt. %	At. %
Ni	24.93	21.95
Ti	23.88	25.77
V	50.79	51.52
O	0	0

It was observed that the amount of titanium decreases in the fusion zone with Vanadium. In the HAZ, the amount of Vanadium increases, and further increment is observed in the amount of Vanadium in the fusion zone. The amount of Aluminum stays the same across the HAZ and parent material (Ti6Al4V). There are no traces of any other elements in the center of interlayer (Vanadium) implying that Vanadium acted as the perfect diffusion barrier between the two base alloys.

Zone 3 and 4 (Ni-Ti-V) HAZ has the similar proportion of Vanadium, Nickel, and Titanium. However, it is interesting to notice the significant increment of Vanadium at the end of HAZ. The presence of Vanadium significantly decreases after the HAZs. The fusion of interlayer (Vanadium) with Ni-Ti and Ti6Al4V also brings some changes in the hardness

across the region. Therefore, the nanoindentation is also performed to determine the hardness across the HAZs of different sides.

4.2.3 Nanoindentation results for samples with Vanadium interlayer.

The hardness of the HAZs of Ni-Ti and Ti6Al4V and the interlayer was the subject of interest to understand the mechanical properties of the weld. The hardness test was conducted in the different regions to ensure the mechanical behavior of various regions could be properly understood. Figure 4.2.7 depicts the regions where the hardness test was performed. Additionally, 4.2.9 is the graphical representation of change in hardness in different zones. The hardness values are tabulated in table 4.2-3.

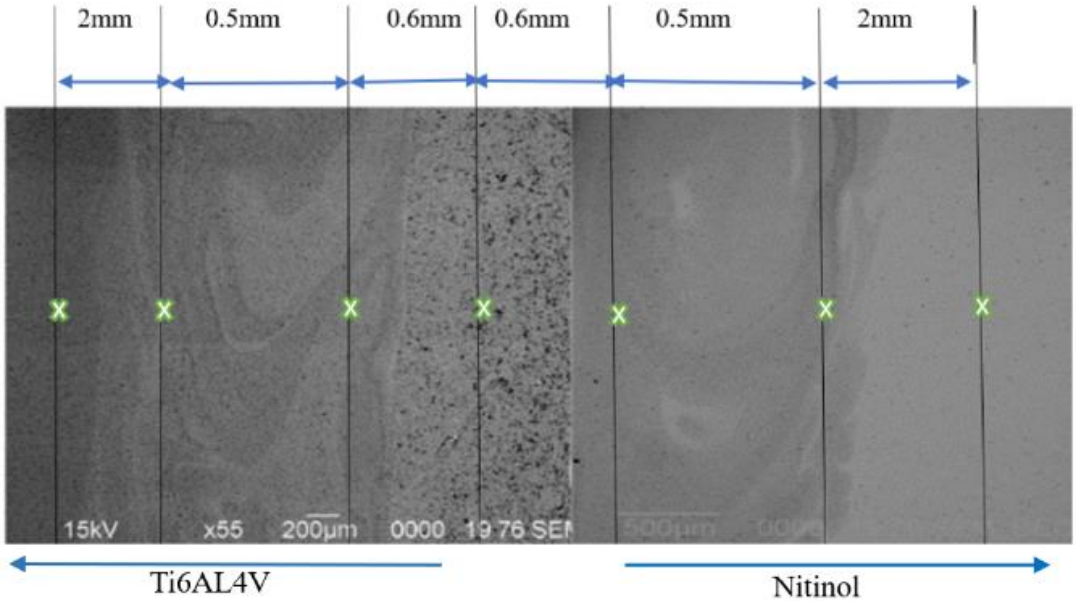

Figure 4.2.7: Regions where Hardness test was performed.

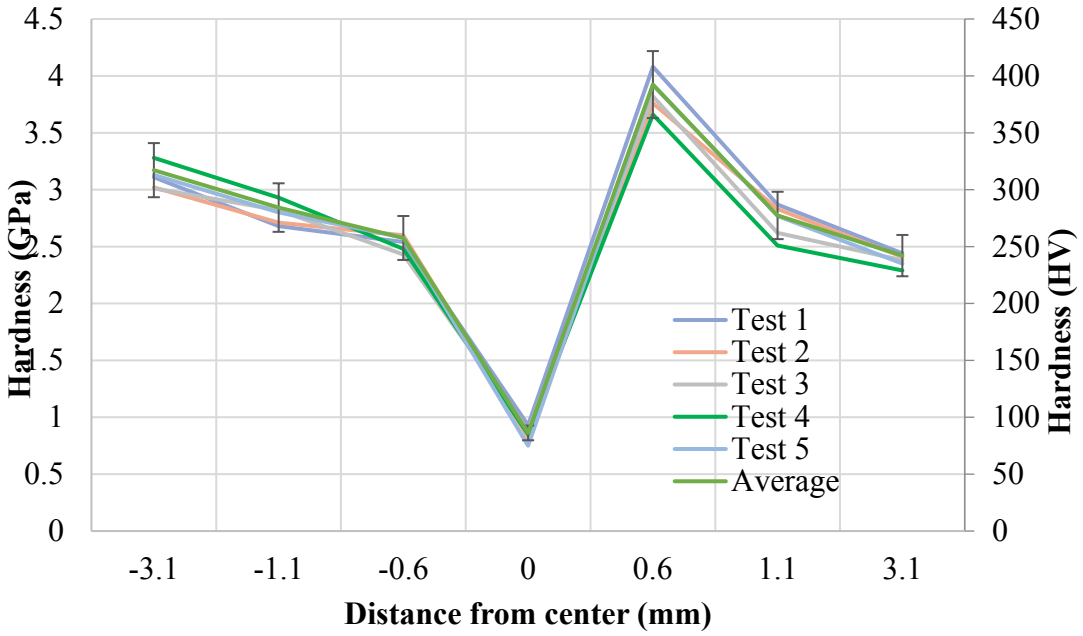

Figure 4.2.8: Change of hardness in different region.

Table 4.2-3:Hardness in different zones

Hardness (GPa)								
	Distance(mm)	Test 1	Test 2	Test 3	Test 4	Test 5	Average	SD
Ti6-4	-3.1	3.11	3.02	3.012	3.28	3.13	3.11	0.10
Ti6-4 HAZ	-1.1	2.68	2.71	2.82	2.93	2.8	2.79	0.09
HAZ close	-0.6	2.54	2.6	2.43	2.48	3	2.53	0.06
Vanadium	0	0.93	0.82	0.88	0.85	0.75	0.85	0.06
NiTi -V HAZ	0.6	4.08	3.76	3.82	3.66	3.92	3.85	0.14
Ni-Ti HAZ	1.1	2.87	2.83	2.62	2.51	2.77	2.72	0.14
Ni-Ti	3.1	2.44	2.41	2.38	2.29	2.35	2.37	0.05

The hardness of Ni-Ti HAZ close to Vanadium interlayer was found to have the highest hardness with an average value of 3.84 GPa. The test performed showed the decrement of hardness in the HAZ of Ti6Al4V interface and increment in Ni-Ti interface. All the tests performed had a similar trend line suggesting the accuracy of the result. The reliability of the hardness testing was validated by the comparison of Ti6Al4V and Nitinol with literature reviews. Also, all the hardness values fall with the 7.5 percentage error of the average values Vanadium has the lowest hardness of all because it is a softer metal.

4.3 Niobium Interlayer sample Analysis

4.3.1 Tensile test and elongation for samples with Niobium interlayer

The samples with Niobium interlayer were subjected to tensile testing based on ASTM E8 standard. All the samples followed a similar trendline, however not all the samples had the same tensile strength. Figure 4.3.1 depicts the stress strain curve for the samples with Nb interlayer and figure 4.3.2 illustrates the maximum strength for the different samples in a bar graph. The maximum values of stress and strain are tabulated in table 4.3-1.

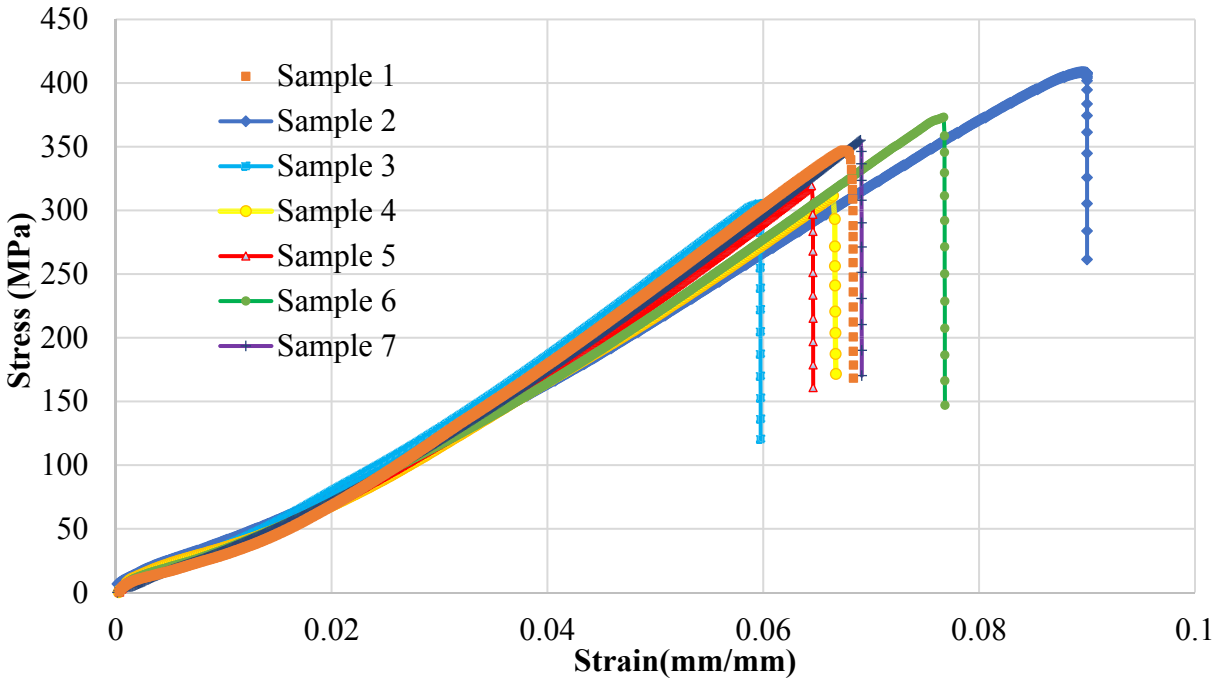

Figure 4.3.1: Stress vs Strain curve for sample with Nb interlayer

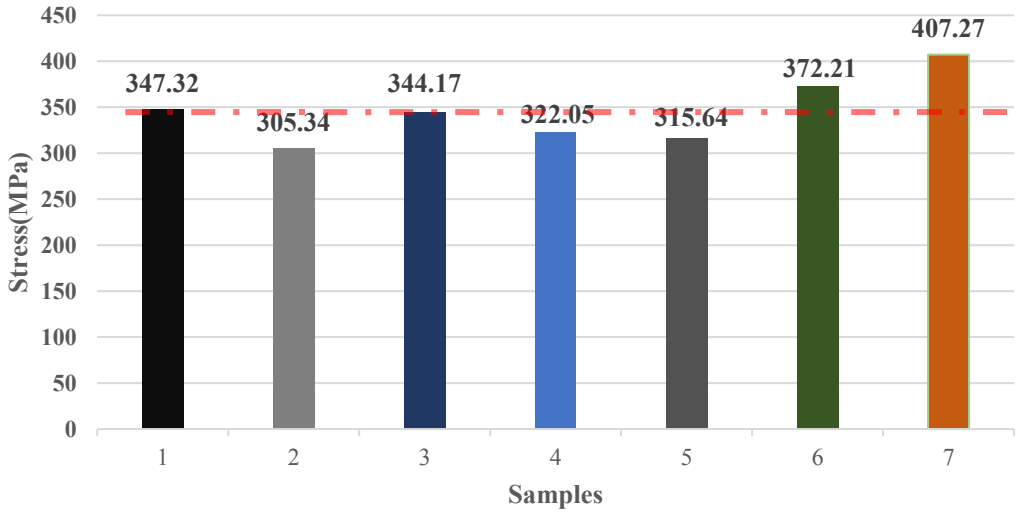

Figure 4.3.2: Maximum tensile strength of Nb interlayer samples

Table 4.3-1: Maximum stress and strain values

Samples	Stress (Mpa)	Strain (%)
1	347.32	6.7
2	305.34	6.0
3	344.17	6.8
4	322.05	6.4
5	315.64	6.6
6	372.21	7.6
7	407.27	8.8
Average	**344.86**	**7**
SD	**32.92**	**0.83**

The range of maximum strength for the samples welded with Nb interlayer 305 MPa to 407 MPa and the range of the strain was 0.0595 to 0.0887. The reason for having such a wide range of strain would be the very subtle and unknown human errors during the any steps of the welding process. The fracture was observed to be brittle and was observed

in the HAZ region of Ni-Ti as well. Figure 4.3.3 shows the broken sample after tensile test.

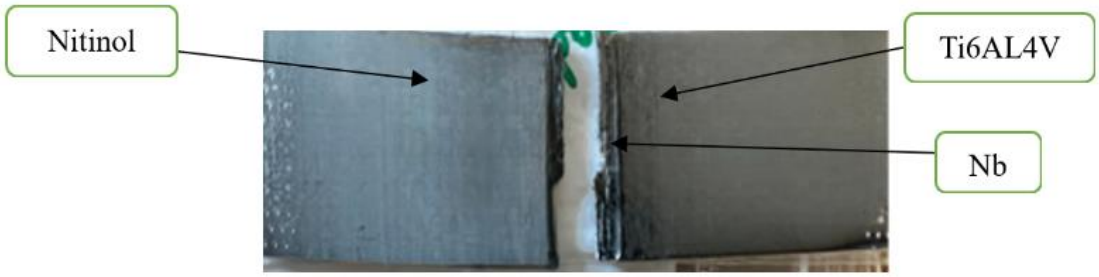

Figure 4.3.3: Broken Nb interlayer sample after tensile test

The Nb interlayer can be seen attached to Ti6Al4V side and the crack is seen in the welded zone between Ni-Ti and the interlayer. Further study of the fracture region is done by SEM analysis of the samples.

4.3.2 Microstructure results for samples with Niobium interlayer

SEM image was taken for the better representation of the fracture region of the weld. Figure 4.3.4 illustrates the fracture that occurred after the tensile test of the samples.

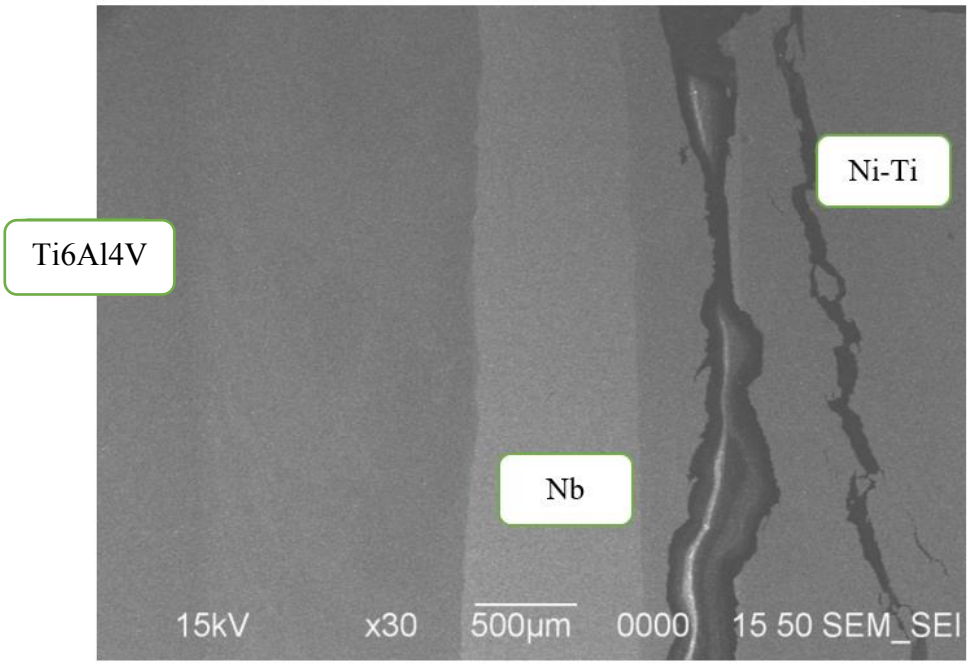

Figure 4.3.4:SEM fracture image after tensile test

SEM analysis also depicted that the HAZ region of the Ni-Ti had several cracks after the tensile test. The HAZ of the Ti6Al4V is not affected by the tensile force applied. Niobium is properly attached to the parent materials forming crack free weld. Niobium also did not melt during the welding process. This prevented the Ni-Ti and Ti6Al4V to fuse and form transverse cracks and brittle intermetallic phases in the weld. Higher magnification imaged were captured for the better understanding of the HAZs in both sides. Figure 4.3.5 illustrates the different patterns formed on both sides during the welding process.

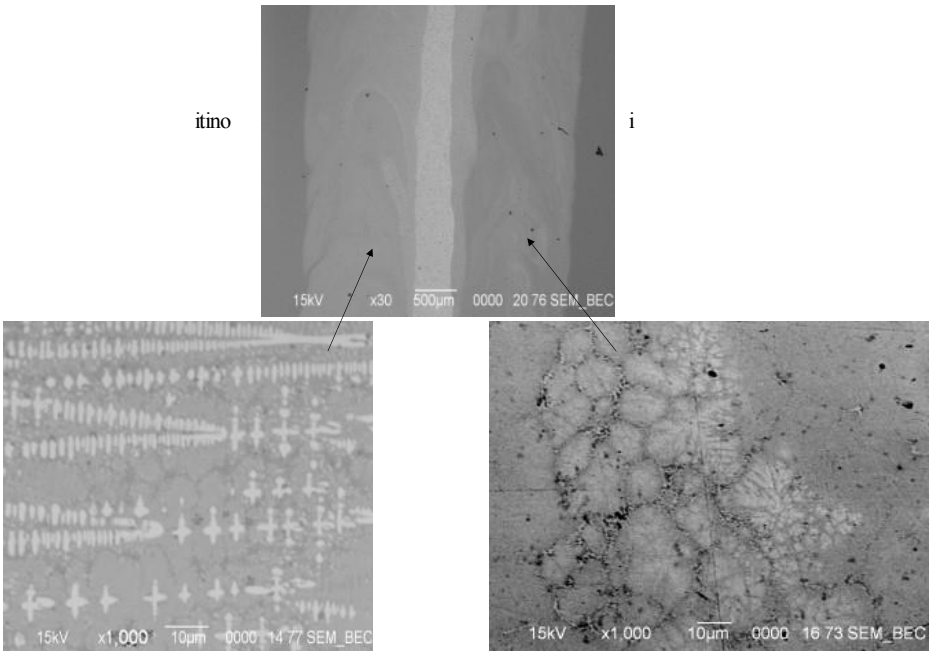

Figure 4.3.5: SEM images for welded region for Nb interlayer sample

Ni-Ti side saw the formation of dendritic structure all over the region. Two phases are formed in the Ni-Ti side due to the exposure to high temperature. Ni-Ti is shaped like a memory alloy; it changes from martensite to austenite when heated and regains its martensite phase when cooled down. When subjected to higher temperature dendrites made up of brittle Ti2Ni are formed [5].

Similarly, the two phases of Ti6Al4V can also be observed on the right side. The heat input the welding caused the phase change in the Ti6Al4V resulting in two phases. The phases formed are stronger in comparison to the dendritic structure formed in the Ni-Ti HAZ.

The elemental composition analysis was done in the HAZ s to find out how the element disperses in the welded sample. The EDS analysis shown in figure 4.3.6 depicts the elements present in the HAZs of both alloys.

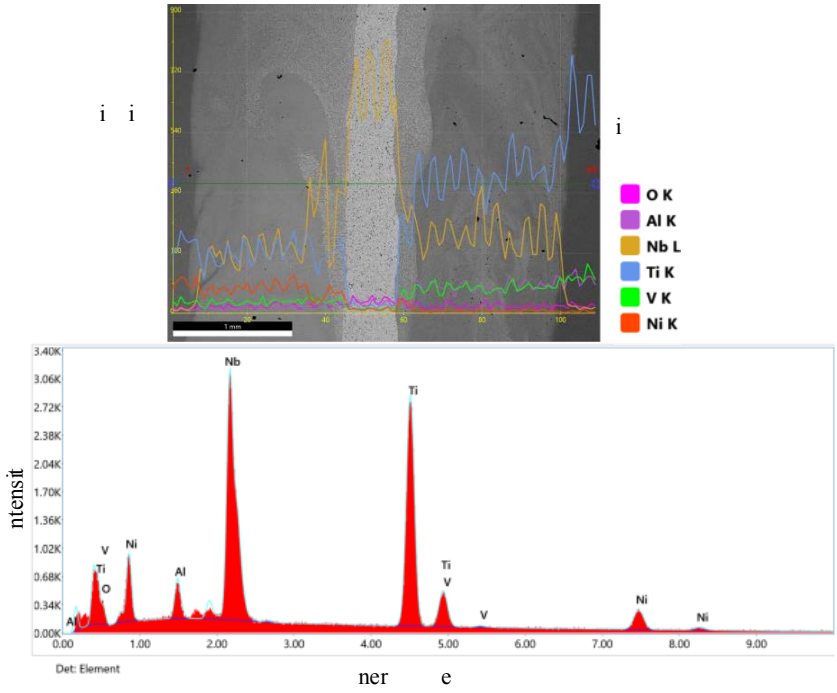

Figure 4.3.6: EDS analysis for the Nb interlayer sample

The left side shows the HAZ of the Ni-Ti where the fusion of Niobium takes place. This zone is dominated by the presence of Niobium and Titanium. Further right advancement towards Nb interlayer increases the presence of Niobium. Hence during the welding process, both Niobium and Ni-Ti fused and caused the formation of Nb rich region.

Only a few parts of the Niobium were fused to two alloys during welding. The HAZ of Ti6Al4V has the highest presence of Titanium followed by Niobium. Aluminum and Vanadium are present in very few amounts. Table 4.3-2 illustrates the wt. % of the element in the region shown in figure 4.3.4.

Table 4.3-2: Elemental composition in Nb interlayer sample

Zone 1		
Elements	Wt. %	At. %
Ni	43.11	40.81
Ti	35.29	37.65
Nb	21.57	22.83
O	0	0

Zone 2		
Elements	Wt. %	At. %
Ni	44.11	38.72
Ti	36.29	37.12
Nb	16.54	15.2
O	3.12	11.38

Zone 3		
Elements	Wt. %	At. %
Al	2.98	2.63
Ti	78.05	75.81
V	2.48	1.16
Nb	15.31	13.92
O	1.79	7.65

Zone 4		
Elements	Wt. %	At. %
Al	3.01	2.63
Ti	80.38	83.15
V	3.12	2.23
Nb	13.64	12.15
O	0	0

Elemental composition of the different region shows that there is very low presence of oxygen in across the interlayer and in the fusion zone. The argon gas flow was successful in preventing the oxidation as there was very less presence of oxygen in the welding region. Due to the various elemental composition in the different regions, there is a change in hardness as well which was further analyzed by hardness test of the samples.

4.3.3 Hardness results for samples with Niobium interlayer.

The hardness of different regions with different elements was performed with nanoindentation technique. Change of mechanical properties due to fusion of different elements and heat input across the different regions was observed. Figure 4.3.7 depicts the figure of different regions where hardness was performed followed by figure 4.3.8 illustrating the different hardness values in different zones. The hardness values are then tabulated in table 4.3-3.

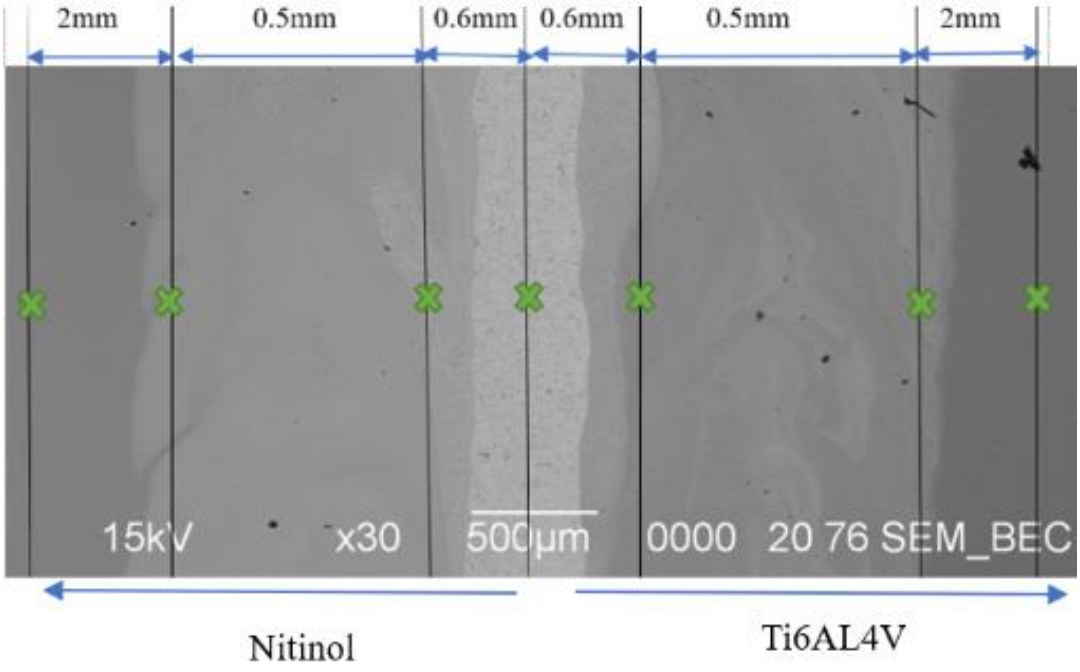

Figure 4.3.7: Hardness test in different regions

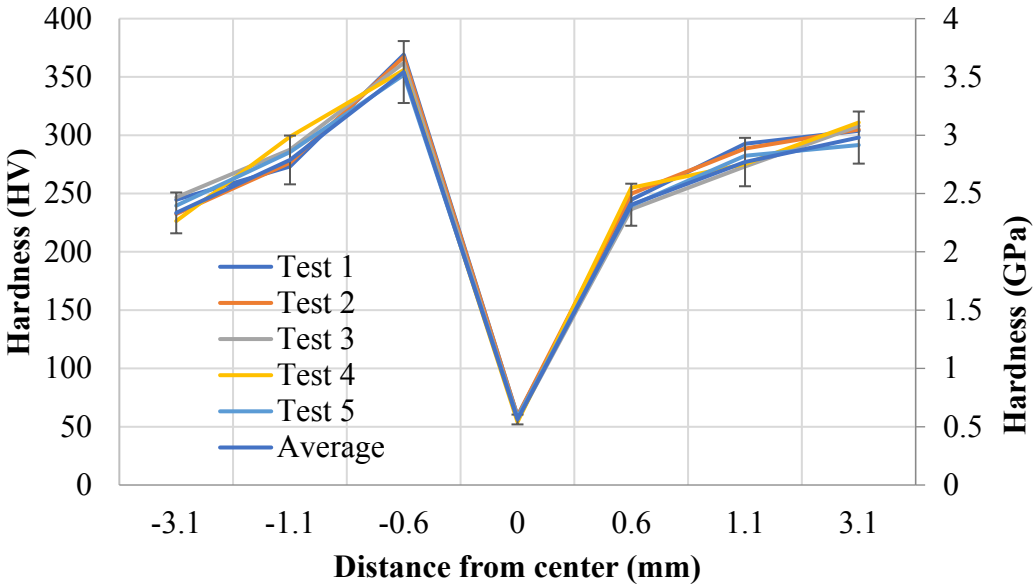

Figure 4.3.8: Hardness values in different region

Table 4.3-3: Hardness in different zones

Hardness (GPa)								
Zones	Distance(mm)	Test 1	Test 2	Test 3	Test 4	Test 5	Average	SD
Ni-Ti	-3.1	2.47	2.28	2.42	2.22	2.35	2.348	0.083
Ni-Ti HAZ	-1.1	2.68	2.71	2.82	2.93	2.8	2.788	0.081
Ni-Ti -Nb HAZ	-0.6	3.62	3.6	3.55	3.32	3.45	3.508	0.10
Nb	0	0.58	0.58	0.55	0.53	0.57	0.562	0.012
Ti6Al4V-Nb HAZ	0.6	2.4	2.45	2.32	2.5	2.35	2.404	0.060
Ti6Al4V HAZ	1.1	2.87	2.83	2.68	2.7	2.77	2.77	0.066
Ti6Al4V	3.1	2.98	2.99	3.02	3.05	3.1	3.028	0.059

The hardness values of the materials were found to be different in all the zones. The reliability of the hardness testing was validated by the comparison of base metal alloys with the previous research. Also, all the hardness values fall with the 7-percentage error of the average values. The HAZ zone of Ni-Ti close to Niobium interlayer is the hardest region among all the regions with an average hardness of 3.508 GPa. The Niobium surface had the lowest hardness value of all with the average value of 0.562 GPa. The fusion of Niobium with Ti6Al4V showed decrement in hardness which is further discussed in the discussion section.

4.4 Discussion of the results

The present study compares and analyzes the experimental results obtained using various interlayers with previous findings from the literature. While earlier studies have explored interlayers consisting of Niobium and Vanadium, the current research employed distinct parameters and equipment, rendering a direct comparison challenging. Nevertheless, this discussion will delve into the reasons underlying the results obtained.

4.4.1 Effects of different interlayer on Tensile test

The tensile strength of the samples with Vanadium and Niobium interlayers surpassed that of the preliminary test, which involved Ni-Ti and Ti6Al4V. The earlier welding attempt resulted in joints that were brittle and easily breakable and could be fractured with bare hands. Hence, welding the two materials with both interlayers, achieving strength exceeding 200 MPa, was a significant improvement over the previous

attempt. The variation in the sample's stress range was due to the manual tasks involved in sample preparation, interlayer insertion, and precise beam positioning on the samples. Despite careful execution, samples with identical strength could not be produced. The average tensile strength of the samples with V Nb are depicted in figure 4.4.1.

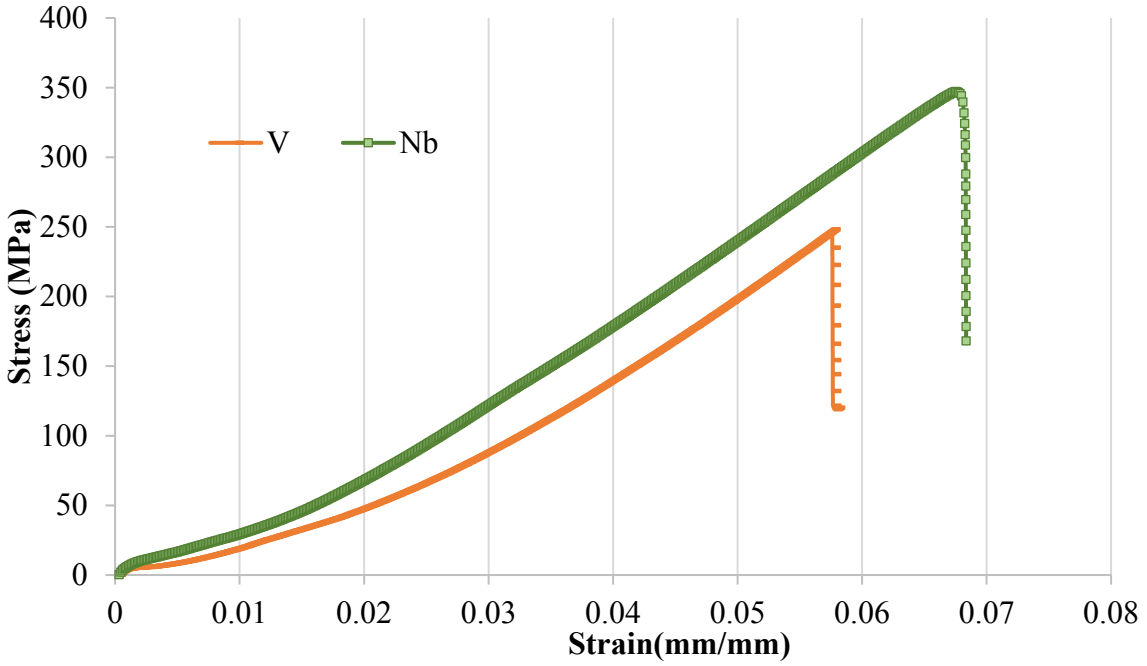

Figure 4.4.1: Tensile strength comparison of V and Nb interlayer samples

The Vanadium interlayer exhibited a strength range of 215MPa to 295MPa, with a crack forming at the welding region interface of V-Ni-Ti. In contrast, Tomaschuk et al. achieved a tensile strength of 367MPa with double-pass welding, joining Ti6Al4V and AISI 316 steel, with fracture occurring in the fusion of V and Ti6Al4V. In our research, the crack appeared in the fusion zone of V and Ni-Ti, and the average tensile strength value

was 63% UTS (251MPa) of annealed Vanadium, in comparison to the 92% UTS from the earlier study [15]. Similarly, welding of Ti6Al4V with 17-PH stainless steel resulted in joint strength of 259 MPa with a fracture in the Fe-Ti interface, using the double-pass technique [47]. These two studies indicate that fusing Ni-Ti with V or its HAZ results in weaker welding joints.

The interlayer samples containing Niobium exhibited significantly higher joint welding strength, with an average of 344 MPa and a tensile strength ranging from 305 MPa to 407 MPa. In contrast, Gao et al. found that the maximum strength obtained during welding of Ti6Al4V and Inconel 718 with a Niobium interlayer was only 145 MPa [46]. Oliveira et al. conducted a tensile test on samples of Ti6Al4V and Ni-Ti, with a cross-section of 2mm^2 and a Niobium interlayer and found an average tensile strength of 300 MPa [14]. The theoretical ultimate strength of the interlayer material is in the range of 250 to 300 MPa [4], which was exceeded by the maximum strength value obtained in our study.

The result obtained with Co and Cu interlayer to join Ni-Ti and Ti6Al4V also depicted a similar result with the tensile strength of in the range of 208-300 MPa of the joints [5, 13]. The welding with Niobium and Vanadium showed good tensile strengths as they are in the similar range with the tests that have been performed. The strength of Niobium interlayer sample has higher strength value than the research by Oliveira [14].

4.4.2 Effect of different interlayers on weld quality and microstructure

Insertion of both interlayer materials exhibited the defect free joint. The microscopic images show that the fusion between the materials took place without any defect. The tensile strength of the samples resulted the fracture in interlayer-Ni-Ti interface. To understand the formation of the different microstructure and chemical composition in fusion zones and HAZs between two materials, SEM and EDS analysis was performed.

In the HAZ of Ti6Al4V and interlayer interface, for the V interlayer samples, two distinctive phases were observed. In the fusion zone with Ti6Al4V, the region is dominated by the presence of Ti-V elements. The defect free region of fusion zone of Ti6Al4V and Vanadium matches with the result obtained by the Tomaschuk and their peers [15]. Similarly, when the V layer was laser deposited over Ti6Al4V, a defect free surface was formed which clarified the compatibility of Ti6Al4V with interlayer [49]. Dissimilar welding between Ti6Al4V and 17-PH exhibited the formation of V- β interface in the fusion zone [47]. In the fusion zone of Ni-Ti and Vanadium, there is a high presence of Vanadium and Titanium, followed by Ni-Ti. This also prevents the formation of transverse cracks in the region [14]. Ni-Ti HAZ region is full of columnar dendrites structure. Vanadium and Nickel rich dendritic region causes the increment in the hardness.

Similar crack free results were observed with the Nb interlayer samples as well as with the improvement in the tensile strength. Both Ti6Al4V-Nb and Ni-Ti-Nb zones are

well fused together which proves that Niobium is also compatible with both materials. In Ti6Al4V-Nb region, dark and light phase patterns. The area is characterized by a prevalence of Titanium and Niobium, with Niobium, as the heavier element, exhibiting a lighter phase and Titanium representing the darker phase. The presence of Aluminum and Vanadium in this region also suggests a composition like some TiNb-based alloys [50, 51]. dditi on of b to these a o s contributes to so id state stren theni n and β stabi ization [52]. In the Ni-Ti- Nb interface, the dendritic kind of structure was seen. According to [45], increment in laser power causes increment in the sizes of dendrites and increment in Nb in both light and dark phases and decrement in Ni amount. They also stated that there is not going to be a change in the microstructure. The dark phases consisted of Ni2Ti in small amounts making this region brittle [14]. This explains the reason behind the brittle fracture in the Ni-Ti -Nb fusion zone.

4.4.3 Effect of different interlayers on hardness

The hardness for the Nb interlayer sample and V interlayer samples shows a similar kind of trend with a slight change in hardness values. The hardness of the fracture region was found to be much higher than that of the other region which explains the fracture of the region. Figure 4.4.2 compares the average hardness of V and Nb interlayer samples in different zones.

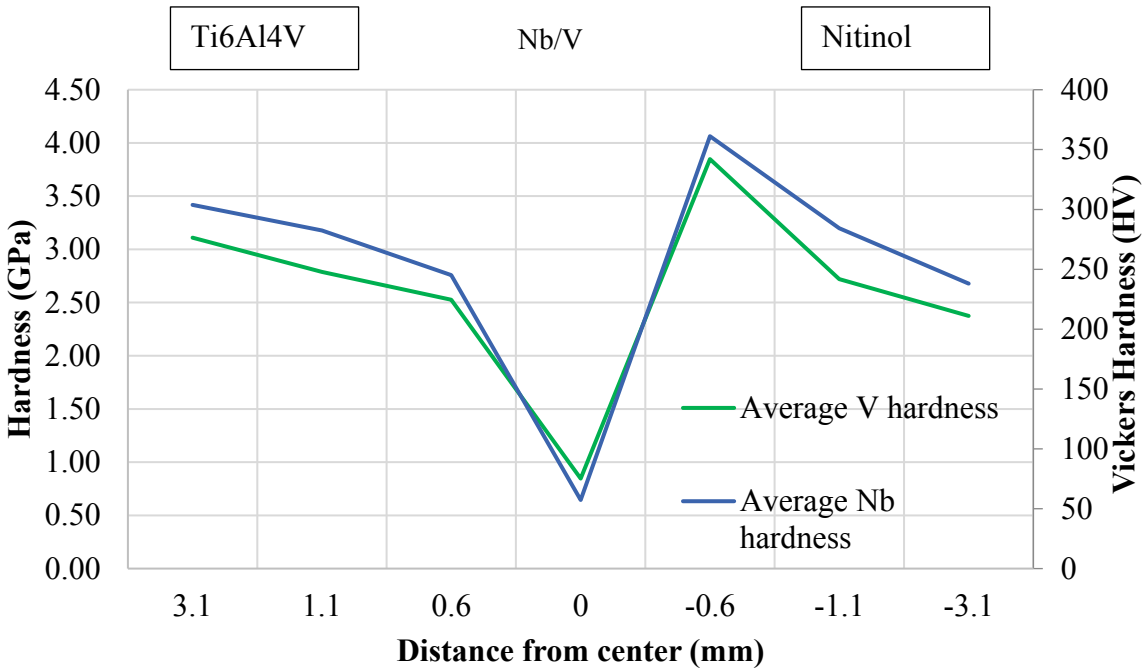

Figure 4.4.2: Hardness values comparison

In V interlayer samples, the hardness of the HAZ of Ti6Al4V decreases as we move towards the fusion zone. The average hardness of the HAZ region close to Ti6Al4V is 2.79 GPa which further decreases to 2.53 GPa in the Ti6Al4V-V zone. The study performed by Adomako et.al saw decrement in the hardness in the melt zone of Vanadium and Ti6Al4V as compared to parent material Ti6Al4V when continuous laser was used [47]. When the double pass technique was used the average value of hardness in the Ti6Al4V-V interface was found to have the average hardness value of 254 HV (2.49 GPa) [47]. They further saw a decrease in hardness of Vanadium with the value of 79 HV (0.77 GPa). This result resembles the results obtained from our experiment where the value of V interlayer was found to have hardness of 0.85 GPa. It was interesting to notice the decrement in hardness

in those regions. Regions with high amounts of Titanium and Vanadium saw a decrease in hardness. However, the HAZ and fusion zone of Nitinol saw increment of hardness. The region has a hardness of 3.8 GPa. The hardness of NiTi increased with the addition of Vanadium [55]. Also, the dark spots observed consist of brittle phases Ni2Ti explaining the reason of fracture in the region [55].

The microhardness test of the Nb interlayer samples shows similar results with increased hardness in the Nitinol HAZ and decreased hardness in Ti6Al4V HAZ. The hardness in the HAZ region of Ti6Al4V decreased from 2.77 GPa to 2.40 GPa as we moved towards Niobium. The hardness results are close to the results obtained by Gao et. al. which was obtained while joining Ti6Al4V with Inconel 718b. The average hardness of the region was 261 HV (2.56 GPa) [46]. The hardness of the niobium region was found to be lowest with the value of 0.56 GPa and the values obtained by Gao et. al. was 70-90 HV (0.68 to 0.88 GPa) [46]. High heat input in our research is the reason behind the Nb having lower hardness. The Nitinol- Nb region has the largest hardness value with 3.508 GPa. The formation of Ni- Nb compounds leads to increased hardness in the region [46].

Chapter 5 Conclusion

5.1 Summary of research findings

Welding of Ti6Al4V and Ni-Ti with Vanadium and Niobium interlayer was successfully performed, and the following concluding results were obtained.

1. Both V and Nb were great interlayers to join Ti6Al4V and Ni-Ti as they helped in the formation of crack free welding and reduce the brittle phases such as Ti2Ni.
2. Using Vanadium and Niobium interlayer increased the welding strength up to 251 MPa and 344 MPa respectively. Samples with Niobium interlayer were found to have greater tensile strength.
3. Tensile test of the specimens depicted that the sample breaks in the Ni-Ti interlayer welding region due to the formation of brittle dendrites structures.
4. Microstructure formed by the fusion of Vanadium and Ti6Al4V and Ti6Al4V and Niobium caused decrement in the hardness.
5. The hardness of the fusion zone of the Ni-Ti to Vanadium and Ni-Ti to Niobium was found to be the highest with 3.848 and 3.548GPa respectively which explains the embrittlement of the region. The fusion of Niobium and Vanadium to Ti6Al4V causes the change in microstructure causing decrement in hardness in HAZ.

5.2 Future works

Improved welding result with both interlayer materials is a promising start for future research. The welding strength was in the similar range to the other research that

have been conducted with the interlayers. The successful welding with both interlayers opens a doorway to further exploration with various modifications. Attempting the welding with different thickness interlayer materials, optimization of parameters of welding by reducing the heat input, optimization of cooling rate of the welding process are few methods that can be attempted to increase the welding strength of the joints by enhancing the quality of the welds.

Chapter 6 References

[1] J. M. Jani, M. Lear , . Subic, and M. . Gibson, “ revi ew of shape memor a o research, app ications and opportunities,” *Materials in Engineering*, vol. 56, pp. 1078–1113, Apr. 2014, doi: 10.1016/j.matdes.2013.11.084.

[2] . O tsuka and . akeshi ta, “Science and echn o o of Shape-Memory Alloys: ew Deve opments,” *Mrs Bulletin*, vol. 27, no. 2, pp. 91–100, Feb. 2002, doi: 10.1557/mrs2002.43.

[3] C. Leyen and M. Peters, “ it anium and it anium o s ,” *Wiley eBooks*, Jan. 2005, doi: 10.1002/3527602119.

[4] M. M. Quazi *et al.*, “Current research and deve opment status of dissimi ar materia s aser we din of titani um and its a o s, ” *Optics and Laser Technology*, vol. 126, p. 106090, Jun. 2020, doi: 10.1016/j.optlastec.2020.106090.

[5] . S. Z oeram and S. . . . Mousavi , “Laser we din of i –6Al– to iti no ,” *Materials in Engineering*, vol. 61, pp. 185–190, Sep. 2014, doi: 10.1016/j.matdes.2014.04.078.

[6] W. A. Miller *et al.*, “Recent deve opment in aluminum alloys for the automotive industr , ” *Materials Science and Engineering A-structural Materials Properties Microstructure and Processing*, vol. 280, no. 1, pp. 37–49, Mar. 2000, doi: 10.1016/s0921-5093(99)00653-x.

[7] M. Behú ová and . B aba ová, “ um erica Simu ation of e mperature Fie ds during Laser Welding–Brazin of / i P a tes,” *Materials*, vol. 16, no. 6, p. 2258, Mar. 2023, doi: 10.3390/ma16062258.

[8] D. Wallerstein *et al.*, “Recent Deve opments in Laser We din of um inum o s to Stee ,” *Metals*, vol. 11, no. 4, p. 622, Apr. 2021, doi: 10.3390/met11040622.

[9] S. ata am a, “ ntroduction: fundamenta s of aser we din ,” *Elsevier eBooks*, pp. 3–16, Jan. 2013, doi: 10.1533/9780857098771.1.3.

[10] E. Akman, A. Demir, T. Canel, and T. Sinmazçe ik, “Laser we din of Ti6Al4V titanium a o s,” *Journal of Materials Processing Technology*, vol. 209, no. 8, pp. 3705–3713, Apr. 2009, doi: 10.1016/j.jmatprotec.2008.08.026.

[11] A. U. Rehman, N. K. Babu, M. K. Talari, Y. S. Usmani, and H. Alkhalefah, “Microstructure and Mechanica Properties of Dissimi ar Friction We din i - 6Al- o to it ino ,” *DOAJ (DOAJ: Directory of Open Access Journals)*, Jan. 2021, doi: 10.3390/met11010109.

[12] . S. Z oeram and S. . . . Mousavi , “ f fect of inter a er thi ckness on microstructure and mechanical properties of as welded Ti6Al4V/Cu/ i i joints,” *Materials Letters*, vol. 133, pp. 5–8, Oct. 2014, doi: 10.1016/j.matlet.2014.06.141.

[13] F. B. Teshome *et al.*, “Microstructure, Macrose r e a tion, and Mechanica Properties of NiTi to Ti6Al4V Dissimi ar Laser We ds Usin C o nter a er ,” *Journal of Materials Engineering and Performance*, vol. 31, no. 12, pp. 9777–9790, Jun. 2022, doi: 10.1007/s11665-022-07064-0.

[14] J. V. Oliveira *et al.*, “Laser joinin of i i t o Ti6Al4V using a Niobium inter a e r,” *Acta Materialia*, vol. 105, pp. 9–15, Feb. 2016, doi: 10.1016/j.actamat.2015.12.021.

[15] . oma shchuk, D. Greve , and P. Sa amand, “Dissimi ar aser we din of S 316L stainless steel to Ti6–Al4– a o via pure vanadium inter a e r,” *Materials Science and Engineering A-structural Materials Properties Microstructure and Processing*, vol. 622, pp. 37–45, Jan. 2015, doi: 10.1016/j.msea.2014.10.084.

[16] V. G. Pushin, N. N. Kuranova, E. B. Marchenkova, and . . P ushin, “Desi n and Development of Ti–Ni, Ni–Mn–Ga and Cu–Al–Ni-based Alloys with High and Low emperature Shape Memor ffects,” *Materials*, vol. 12, no. 16, p. 2616, Aug. 2019, doi: 10.3390/ma12162616.

[17] S. Samal, O. Kosjakova, D. okoun, a nd . Stachiv, “Shape Memor Beha viour of PMMA-Coated i i o under herma C c e,” *Polymers*, vol. 14, no. 14, p. 2932, Jul. 2022, doi: 10.3390/polym14142932.

[18] . O tsuka and X. Ren, “Ph si ca meta ur of i–Ni-based shape memory a o s, ” *Progress in Materials Science*, vol. 50, no. 5, pp. 511–678, Jul. 2005, doi: 10.1016/j.pmatsci.2004.10.001.

[19] . J. akahashi, . Sakur ai, S. Watanabe, . Masahashi , and S. Hanada, “ ff ect of Heat Treatment and Sn Content on Superelasticity in Biocompatible TiNbSn o s ,” *Materials Transactions*, vol. 43, no. 12, pp. 2978–2983, Dec. 2002, doi: 10.2320/matertrans.43.2978.

[20] . . uran ova, . . Makarov, . G. Pushin, and Y. Ust u ov, “ nf uence of Heat Treatment and Deformation on the Structure, Phase Transformation, and Mechanical Behavior of Bulk TiNi-Based o s, ” *Metals*, vol. 12, no. 12, p. 2188, Dec. 2022, doi: 10.3390/met12122188.

[21] L. Qian, X. Xiao, Q. Sun, and . Y u, “ noma ous re ationship between hardness and wear properties of a superelastic nickel–titanium a o ,” *Applied Physics Letters*, vol. 84, no. 7, pp. 1076–1078, Feb. 2004, doi: 10.1063/1.1646218.

[22] M. D. . Ferreira, M. . Luersen, and P. a. . Bor e s, “ ic ke -titanium alloys: a s st ematic review,” *Dental Press Journal of Orthodontics*, vol. 17, no. 3, pp. 71–82, Jun. 2012, doi: 10.1590/s2176-94512012000300016.

[23] M. Ba asubramanian, R. Srimath, L. i nesh, a nd S. Rajesh, “ pp i cation of shape memory alloys in engineering – revi ew,” *Journal of Physics*, vol. 2054, no. 1, p. 012078, Oct. 2021, doi: 10.1088/1742-6596/2054/1/012078.

[24] M. ii nomi, “Mechanica properties of biomedica titanium a o s,” *Materials Science and Engineering A-structural Materials Properties Microstructure and Processing*, vol. 243, no. 1–2, pp. 231–236, Mar. 1998, doi: 10.1016/s0921-5093(97)00806-x.

[25] M. Boivineau *et al.*, “ h ermoph s ica Properties of So id and Liquid i -6Al-4V o ,” *International Journal of Thermophysics*, vol. 27, no. 2, pp. 507–529, Mar. 2006, doi: 10.1007/pl00021868.

[26] Y.-J. Lee, M. D. Peters, and G. Wirth, “ ff ects of thermomechanical treatment on microstructure and mechanical properties of blended elemental Ti-6Al-4V

compacts," *Materials Science and Engineering A-structural Materials Properties Microstructure and Processing*, vol. 102, no. 1, pp. 105–114, Jun. 1988, doi: 10.1016/0025-5416(88)90538-1.

[27] J. E. Fuchs, J. S. Goldstein, and D. J. Stephenson, "Mechanical Properties Data for Several High-Strength Alloys", NASA Technical Note D-555, 1960.

[28] . M. B eese and B. Carro , "Review of Mechanica Properties of i -6Al-4V Made by Laser-Based dditive Manufacturin U sin Powder F eedstock," *JOM*, vol. 68, no. 3, pp. 724–734, Mar. 2016, doi: 10.1007/s11837-015-1759-z.

[29] M. azem i, S. han arani , M. sm ai ian, and . Shana hi, " nvesti atio n on the corrosion behavior and biocompatibility of Ti-6Al-4V implant coated with H / i dua a er for medica app ic ations," *Surface & Coatings Technology*, vol. 397, p. 126044, Sep. 2020, doi: 10.1016/j.surfcoat.2020.126044.

[30] F. . F eninat, G. Laroche, M. Fiset, and D. Mantovani, "Shape Memor Materia s for Biomedica pp ications," *Advanced Engineering Materials*, vol. 4, no. 3, pp. 91–104, Mar. 2002, doi: 10.1002/1527-2648(200203)4:3.

[31] A. Falanga *et al.*, " iob ium-Treated Titanium Implants with Improved Cellular and Molecular Activities at the Tissue– mp ant nterface," *Materials*, vol. 12, no. 23, p. 3861, Nov. 2019, doi: 10.3390/ma12233861.

[32] W. G. Ha nes, " CRC Handbook of Chemistr a nd Ph sics," *CRC Press eBooks*, Jun. 2014, doi: 10.1201/b17118.

[33] CRC Handbook of Chemistry and Physics. (2019). 100th Edition. Taylor & Francis Group.

[34] J. Carvi , “Mechanica n ineer’s D ata Handbook,” *Elsevier eBooks*, Jan. 1993, doi: 10.1016/c2009-0-24207-3.

[35] Trivedi, Y. N. (2019). Investigation of Mechanical Properties of Bulk and Additively Manufactured Ni-Mn-Ga Shape Memory Alloy using Nanoindentation and Microhardness Techniques [Master's thesis, Youngstown State University]. OhioLINK Electronic Theses and Dissertations Center. http://rave.ohiolink.edu/etdc/view?acc_num=ysu155865619144072

[36] Fischer-Cripps, A. C. (2002). Nanoindentation. Springer, New York, NY. doi: 10.1007/978-0-387-22458-7

[37] Ferraro, M. M. (2018). Quantitative Determination of Residual Stress on Additively Manufactured Ti-6Al-4V [Master's thesis, Youngstown State University]. OhioLINK Electronic Theses and Dissertations Center. http://rave.ohiolink.edu/etdc/view?acc_num=ysu152640278957619

[38] W. Guo, Y. Chen, Y. Huang, Y. Mao, and Y.-Y. Yu, “ ff ects of niobium addition on the microstructure and mechanical properties of laser-welded joints of NiTiNb and Ti6Al4V a o s,” *Journal of Alloys and Compounds*, vol. 735, pp. 2616–2624, Feb. 2018, doi: 10.1016/j.jallcom.2017.11.307.

[39] A. W. Glaspell, J. A. D. De La Peña, S. Dahal, S. Neupane, J. K. Ryu, and K. Choo, “Heat ransf er and Structura Characteristics of Dissimi ar Joints Joinin Ti- and i i vi a Laser We din , ” *Energies*, vol. 15, no. 19, p. 6949, Sep. 2022, doi: 10.3390/en15196949.

[40] . C apriccio i and P. Frosi, “Mu tipurpose SYS F procedure for we din processes simu ation,” *Fusion Engineering and Design*, vol. 84, no. 2–6, pp. 546–553, Jun. 2009, doi: 10.1016/j.fusengdes.2009.01.039.

[41] F. B. Teshome *et al.*, “Ro e of Pd inter a er on i i t o Ti6Al4V laser welded joints: microstructura evo ution and stren thenin mec hanisms,” *Materials & Design*, vol. 228, p. 111845, Mar. 2023, doi: 10.1016/j.matdes.2023.111845.

[42] H. Vemanaboina, E. Gundabattini, S. Ake a, and R. . Buddu, “ herm a na si s Simu ation for Laser Butt We din of ncone 5 Usin F ,” *International Journal of Engineering and Technology (UAE)*, vol. 7, no. 4.10, p. 85, Oct. 2018, doi: 10.14419/ijet.v7i4.10.20711.

[43] P. S. Ghosh *et al.*, “Prediction of Transient Temperature Distributions for Laser We din of Dissimi ar Meta s,” *Applied Sciences*, vol. 11, no. 13, p. 5829, Jun. 2021, doi: 10.3390/app11135829.

[44] Mizar, S. (2006). Thermomechanical characterization of Ni-Ti and Ni-Ti based structures using ACES methodology. : Worcester Polytechnic Institute.

[45] Y.-T. Lee, J.-R. Zhuang, W.-H. Hsieh, and A.-S. Yan , “F M Simu ations to Study the Effects of Laser Power and Scan Speed on Molten Pool Size in dditi ve Manufacturin , ” *World Academy of Science, Engineering and Technology, International Journal of Mechanical, Aerospace, Industrial, Mechatronic and Manufacturing Engineering*, vol. 11, no. 7, pp. 1298–1302, May 2017, doi: 10.5281/zenodo.1131063.

[46] X. Gao, J. Liu, and L. Zhan , “Dis simi ar meta we din of Ti6Al4V and Inconel 718 through pulsed laser welding-induced eutectic reaction techno o ,” *The International Journal of Advanced Manufacturing Technology*, vol. 96, no. 1–4, pp. 1061–1071, Feb. 2018, doi: 10.1007/s00170-018-1633-6.

[47] N. K. Adomako, J.-O. Kim, H. M. Lee, K.-H. oh, and J. H. im, “Dis simi ar welding between Ti–6Al–4V and 17-4PH stainless steel using a vanadium inter a e r,” *Materials Science and Engineering A-structural Materials Properties Microstructure and Processing*, vol. 732, pp. 378–397, Aug. 2018, doi: 10.1016/j.msea.2018.07.015.

[48] C. B. Park, N. K. Adomako, M.-G. Lee, J. . im, and J. H. im, “ nter facia structure and pore formation mechanism during laser cladding of pure vanadium on Ti-6Al- a o ,” *International Journal of Refractory Metals & Hard Materials*, vol. 101, p. 105671, Dec. 2021, doi: 10.1016/j.ijrmhm.2021.105671.

[49] Piao, M., Miyazaki, S., Otsuka, K. and Nishida, N., 1992. Effects of Nb addition on the microstructure of Ti–Ni alloys. Materials Transactions, JIM, 33(4), pp.337-345.

[50] Z. A. Liu, J. Lin, S. Li, and G.-M. Chen, “ ff ects of b and on t he microstructures and mechanical properties of high Nb containing TiAl base a o s, ” *Intermetallics*, vol. 10, no. 7, pp. 653–659, Jul. 2002, doi: 10.1016/s0966-9795(02)00037-7.

[51] R.-G. Zhan and . L. cof f, “Processin sheet materia s b accumu ati ve ro bondin a nd reaction annea in from i / / b e e menta foi s,” *Materials Science*

and Engineering A-structural Materials Properties Microstructure and Processing, vol. 463, no. 1–2, pp. 67–73, Aug. 2007, doi: 10.1016/j.msea.2006.06.144.

[52] R. F. Bo er, G. We sch, and . W. Co in s, “Ma teria s Properties Handbook: ita nium o s,” *ASM International*, Dec. 1994.

[53] . Y uan, Y. Wan , L. S. Zhen , and H. Y . Zhan , “Microstructura evo ution, mechanical properties, and oxidation performance of highly Ni-rich NiTi alloys with added usin vacuum arc me tin ,” *Journal of Alloys and Compounds*, vol. 877, p. 160263, Oct. 2021, doi: 10.1016/j.jallcom.2021.160263.

[54] J. Zhu *et al.*, “Contro in mi crostructure evo ution and phase transformation behavior in additive manufacturing of nitinol shape memory alloys by tuning hatch distance,” *Journal of Materials Science*, vol. 57, no. 10, pp. 6066–6084, Mar. 2022, doi: 10.1007/s10853-022-07007-z.

[55] S. Sampath and S. edamani ckam, “ ffe ct of a nadium on the Microstructure, Transformation Temperatures, and Corrosion Behavior of NiTi Shape Memory o s ,” Journa of n ineerin Mat eria s and echno o -transactions of the Asme, vol. 145, no. 1, Oct. 2022, doi: 10.1115/1.4055910.

[56] M. J. Wiegand, L. Marks, N. Sommer, and S. Bohm, “Dissimi ar micro beam welding of titanium to Nitinol and stainless steel using biocompatible filler materia s for medica app ications,” We din in the Wor d, vo . 7, no. 1, pp. 77–88, Nov. 2022, doi: 10.1007/s40194-022-01412-3.

[57] Thurnay, Kalman. Thermal properties of transition metals. Karlsruhe: Forschungszentrum Karlsruhe, 1998.

[58] Shabalin, Igor L., and Igor L. Shabalin. "Niobium." Ultra-High Temperature Materials I: Carbon (Graphene/Graphite) and Refractory Metals (2014): 531-607.